

MiR-135a-5p Is Critical for Exercise-Induced Adult Neurogenesis

Meritxell Pons-Espinal,^{1,6} Caterina Gasperini,^{1,6} Matteo J. Marzi,² Clarissa Braccia,³ Andrea Armirotti,³ Alexandra Pöttsch,^{4,5} Tara L. Walker,^{4,5} Klaus Fabel,^{4,5} Francesco Nicasio,² Gerd Kempermann,^{4,5} and Davide De Pietri Tonelli^{1,*}

¹Neurobiology of miRNA, Istituto Italiano di Tecnologia (IIT), Genoa, Italy

²Center for Genomic Science of IIT@SEMM, Istituto Italiano di Tecnologia (IIT), Milan, Italy

³Analytical Chemistry Facility, Istituto Italiano di Tecnologia (IIT), Genoa, Italy

⁴German Center for Neurodegenerative Diseases (DZNE) Dresden, Dresden, Germany

⁵CRTD – Center for Regenerative Therapies, Technische Universität Dresden, Dresden, Germany

⁶Co-first author

*Correspondence: davide.depietri@iit.it

<https://doi.org/10.1016/j.stemcr.2019.04.020>

SUMMARY

Physical exercise stimulates adult hippocampal neurogenesis and is considered a relevant strategy for preventing age-related cognitive decline in humans. The underlying mechanisms remains controversial. Here, we show that exercise increases proliferation of neural precursor cells (NPCs) of the mouse dentate gyrus (DG) via downregulation of microRNA 135a-5p (miR-135a). MiR-135a inhibition stimulates NPC proliferation leading to increased neurogenesis, but not astrogliogenesis, in DG of resting mice, and intriguingly it re-activates NPC proliferation in aged mice. We identify 17 proteins (11 putative targets) modulated by miR-135 in NPCs. Of note, inositol 1,4,5-trisphosphate (IP3) receptor 1 and inositol polyphosphate-4-phosphatase type I are among the modulated proteins, suggesting that IP3 signaling may act downstream miR-135. miR-135 is the first noncoding RNA essential modulator of the brain's response to physical exercise. Prospectively, the miR-135-IP3 axis might represent a novel target of therapeutic intervention to prevent pathological brain aging.

INTRODUCTION

In most mammalian species, the postnatal subgranular zone (SGZ) of the hippocampal dentate gyrus (DG) maintains a population of neural precursor cells (NPCs) retaining the lifelong capability to generate new neurons and astrocytes. However, this process inexorably declines with age (Eriksson et al., 1998; Spalding et al., 2013, 2005 and; Knoth et al., 2010; Dennis et al., 2016; Mathews et al., 2017; Kempermann et al., 2018), and this decline has been correlated with the loss of cognitive abilities and the occurrence of several brain pathologies (Bond et al., 2015; Urban and Guillemot, 2014). Currently, many translational concepts for preserving cognitive abilities in the aging brain thus aim at sustaining, or even increasing, the potential for cognitive plasticity and flexibility that is contributed by the adult-generated neurons.

Environmental enrichment and physical activity (e.g., voluntary running in a wheel) potentiate adult neurogenesis in rodents (Farioli-Vecchioli et al., 2014; Fischer et al., 2014; Kronenberg et al., 2006, 2003; Lugert et al., 2010; Overall et al., 2013; van Praag et al., 1999). The positive response of adult neurogenesis to these stimuli is maintained into old age and counteracts the age-associated cognitive decline in rodents and likely in humans (Kempermann et al., 2002, 1998; Kempermann et al., 2018; Kronenberg et al., 2006; van Praag et al., 2005). However, the cellular and molecular

mechanisms underlying homeostasis of adult neurogenesis and its response to environmental stimuli remain elusive (Encinas and Fitzsimons, 2017; Overall et al., 2016). We hypothesize that exploiting these mechanisms is relevant for preventing age-related cognitive decline in humans and that our animal models can contribute to providing evidence-based recommendations for an active lifestyle for successful aging.

The molecular control of adult neurogenesis is highly polygenic (Kempermann, 2011) and very likely regulated at multiple levels, including epigenetic, post-transcriptional as well as post-translational (Encinas and Fitzsimons, 2017; Stricker and Götz, 2018). Single-cell RNA sequencing efforts start to reveal molecular cascades underlying adult neurogenesis (Shin et al., 2015). However, it remains unclear how the subtle changes in transcript abundance can be translated to biologically relevant protein levels. This enormous complexity thus hinders the identification of the proteins and pathways that are at the top of the molecular control of adult neurogenesis and its response to the environment.

MicroRNAs (miRNAs) are small noncoding RNAs which, by post-transcriptional repression of hundreds of target messenger RNAs (mRNAs) in parallel, tune the entire cell proteome (Selbach et al., 2008). The functional synergism of few miRNAs achieves gene regulation essential for proliferation, cell fate determination, and survival in embryonic (Barca-Mayo and De Pietri Tonelli, 2014) and

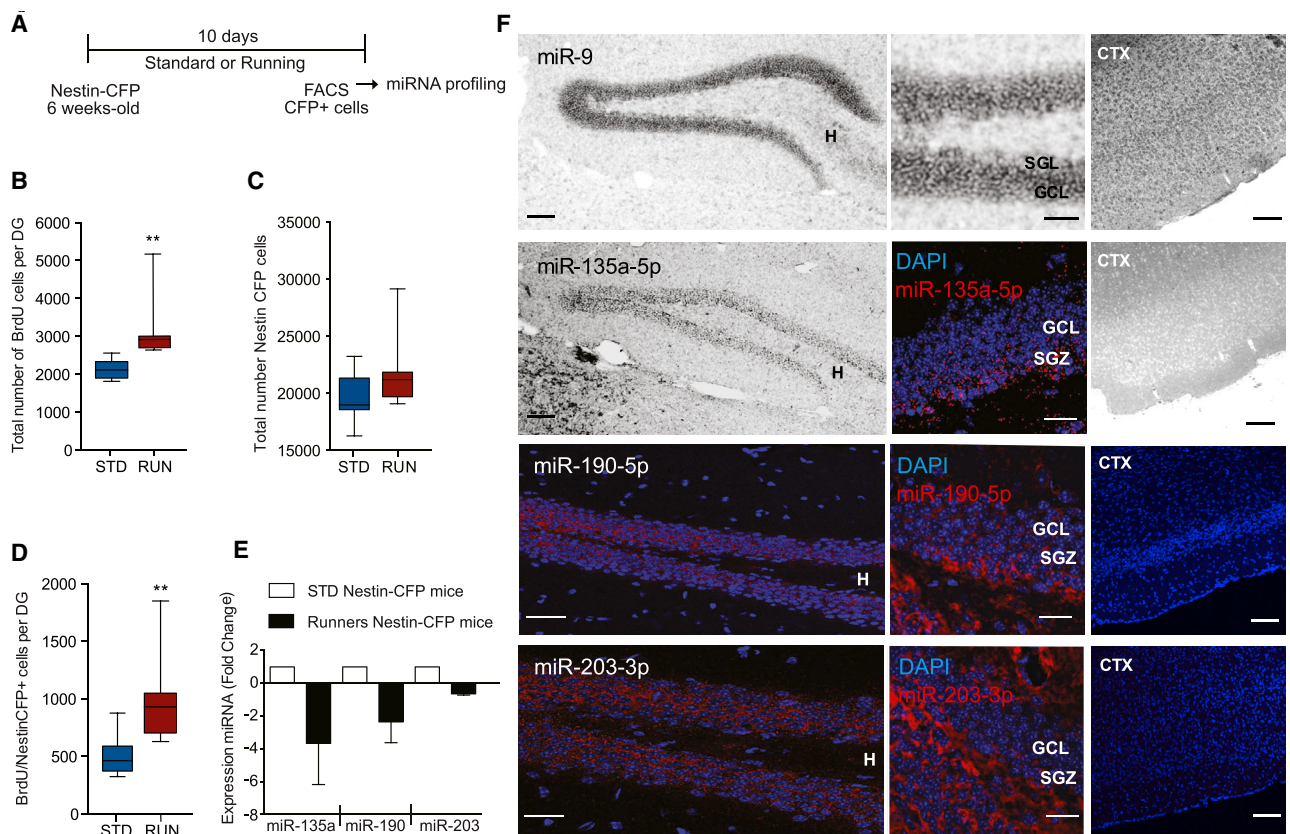


Figure 1. Running-Induced Proliferation Downregulates miRNA Expression in Nestin-Positive Adult Hippocampal NPCs *In Vivo*

(A) Schematic representation of the experiment.

(B–D) (B) Total number of BrdU and (C) *Nestin*-CFPnuc positive adult neural progenitor cells (NPCs), or (D) proportion of BrdU/*Nestin*-CFPnuc double-positive cells counted from the hippocampal SGZ of *Nestin*-CFPnuc mice under standard (STD) or running (RUN) conditions for 10 days; n = 8 mice per group.

(E) Quantification of relative expression levels of miR-135-5p, miR-190-5p, and miR-203-3p by TaqMan low density array (TLDA) in sorted *Nestin*-CFPnuc NPCs from the hippocampus of adult mice in STD or RUN conditions.

(F) Representative micrographs showing expression of miR-9-5p (positive control), miR-135-5p, miR-190-5p, and miR-203-3p by *in situ* hybridization in the DG and cortex (CTX) of 6-week-old C57Bl6J mice. H, hilus, GCL, granular cell layer; SGZ, subgranular zone.

Data are expressed as means ± SEM, n = 3 independent experiments. One-way ANOVA Bonferroni as *post hoc*. **p < 0.01. Scale bar, 100 μm (large panel), 50 μm (small panel).

adult NPCs (Encinas and Fitzsimons, 2017; Pons-Espinal et al., 2017; Stappert et al., 2018). Interestingly, running stimulates hippocampal NPC proliferation (Overall et al., 2016) and alters miRNA expression in rodents (Bao et al., 2014; Cosín-Tomás et al., 2014; Hu et al., 2015; Pan-Vazquez et al., 2015). Hence, we hypothesize that investigating miRNAs involved in running-induced neurogenesis would allow the identification of the most prominent pathways that constrain NPC proliferative potential in the adult mouse hippocampus. With this approach, we aim to uncover the proteins and pathways acting within this circuit-level context, hence providing a system-level biological understanding of scientific and therapeutic value.

RESULTS

Running-Induced Proliferation Downregulates miRNA Expression in Nestin⁺ Adult Hippocampal NPCs *In Vivo*

To investigate whether running alters miRNAs expression in adult hippocampal NPCs, 6-week-old mice, expressing the fluorescent protein CFPnuc under control of the *Nestin* promoter (*Nestin*-CFPnuc), were housed under standard conditions or equipped with a running wheel for 10 days (Figure 1A). As expected, in the hippocampal SGZ of running mice, we found a statistically significant increase in the number of bromodeoxyuridine (BrdU)-positive cells (Figure 1B; p = 0.005) and BrdU/*Nestin*-CFPnuc double-positive NPCs (Figure 1D; p = 0.007), and a slight

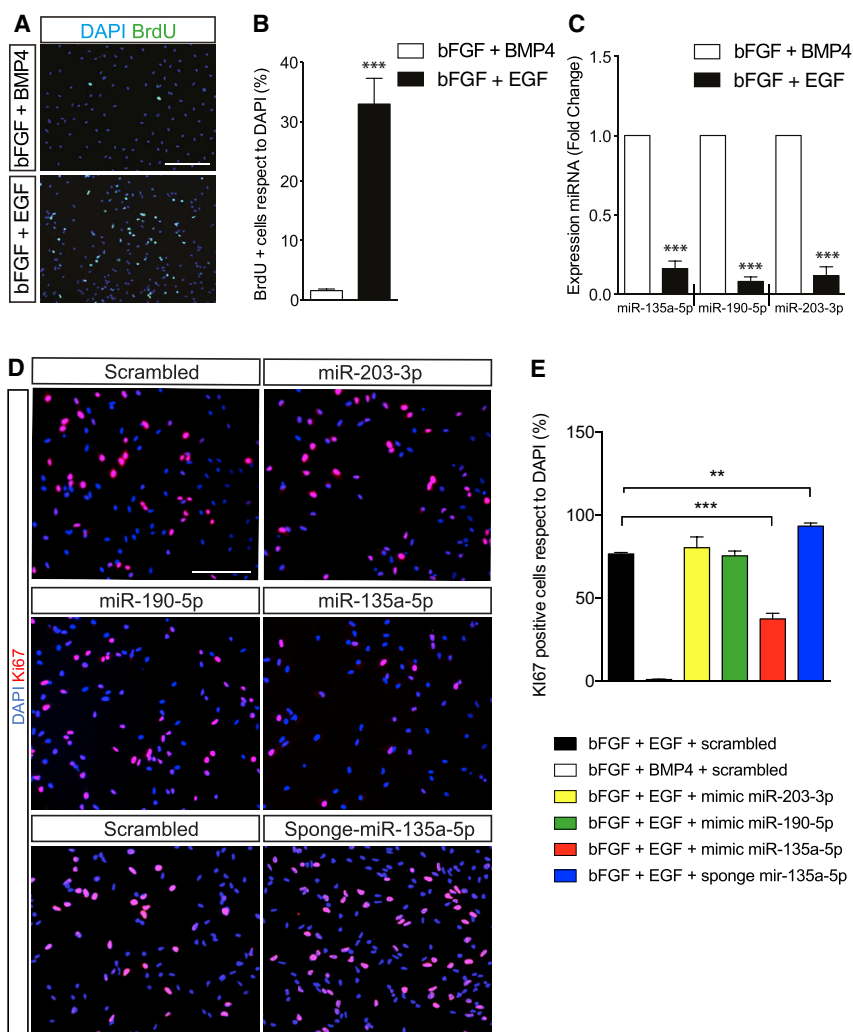


Figure 2. miR-135a Levels in Adult NPCs Are Cell-Cycle Dependent and Its Modulation Affects Cell Proliferation *In Vitro*

(A and B) Representative micrographs showing (A) BrdU-positive and (B) quantification in primary hippocampal adult NPCs cultured in proliferative medium (EGF + bFGF), or quiescence medium (BMP4 + bFGF).

(C) Relative miRNA fold change expression.

(D and E) Representative micrographs showing (D) Ki67-positive NPCs and (E) quantification cultured in proliferative medium (EGF + bFGF) upon transfection with 50 nM scrambled control, miR-203-3p, miR-190-5p, miR-135a-5p mimics, or upon transduction with lentivirus transcribing a sponge for miR-135a (sponge miR-135a, i.e., loss of function) or virus expressing control (scrambled) RNAs.

Data are expressed as means \pm SEM, $n = 3$ independent experiments containing three replicates. One-way ANOVA Bonferroni as *post hoc*. ** $p < 0.01$, *** $p < 0.001$. Scale bars, 50 μ m.

increase (not statistically significant) in the total number of *Nestin*-CFPnuc-positive NPCs (Figure 1C; $p = 0.136$), suggesting an expansion of the proliferative NPC pool.

We sorted *Nestin*-CFPnuc⁺ NPCs from the DG of resting and running mice and found eight miRNAs that were reproducibly downregulated in runners compared with resting mice (Figure S1, TaqMan low density array [TLDA], $n = 3$ independent biological replicates each containing a pool of *Nestin*-CFPnuc⁺ cells isolated from eight mice per condition). Of relevance, none of the miRNAs in the TLDA were reproducibly induced in *Nestin*-CFPnuc⁺ NPC upon running (Table S1). The three most downregulated miRNAs in *Nestin*-CFPnuc⁺ NPCs from the DG of running mice were mmu-miR-135a-5p (miR-135a), mmu-miR-190-5p (miR-190), and mmu-miR-203-3p (miR-203) (Figure 1E). By *in situ* hybridization, we found that expression of these miRNAs was enriched in the DG of adult resting mice (Figure 1F) and that only miR-135a and miR-190 were preferentially enriched in the hippocampal SGZ,

where NPCs are located *in vivo* (Figure 1F). These results indicate that running decreases miRNA expression in hippocampal NPCs *in vivo*, opening the possibility that some of these miRNAs might be involved in the mechanism underlying running-induced proliferation of adult NPCs.

miR-135a Inhibits Cell-Cycle Progression of Cultured Adult NPCs and Mediates Running-Induced Proliferation in the Hippocampal SGZ *In Vivo*

To investigate this possibility, we compared expression of the three miRNAs in cultures of primary hippocampal NPCs (Babu et al., 2011) in quiescence and proliferative conditions. Quiescence is operationally defined here as “non-proliferative” and induced *in vitro* by the addition of bone morphogenetic protein 4 (BMP4, Martynoga et al., 2013) to the culture medium containing fibroblast growth factor 2 (FGF2/bFGF). Proliferation medium was supplemented with both FGF2 and epidermal growth factor (EGF) (Pons-Espinal et al., 2017, Figures 2A–2C). As

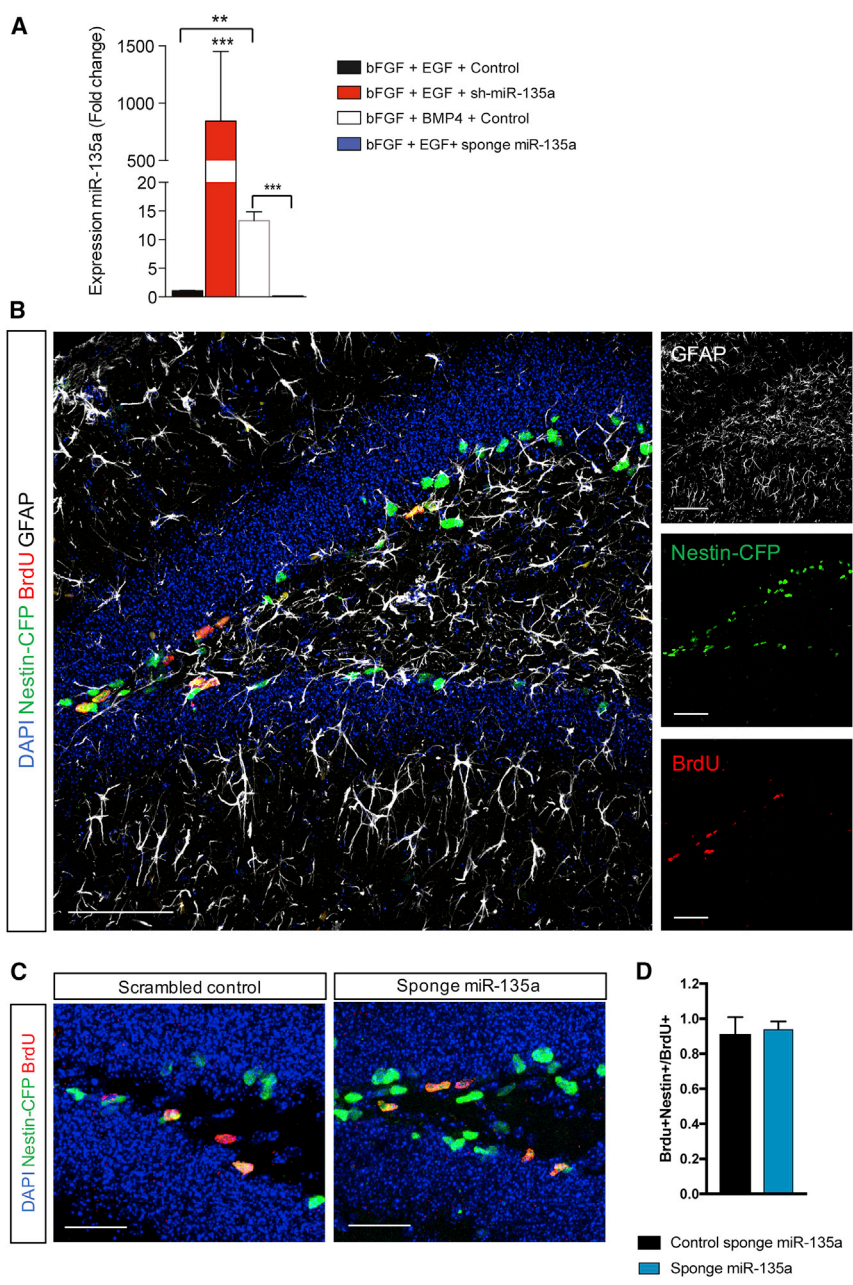


Figure 3. Validation of Lentiviruses to Overexpress/Downregulate miR-135a in NPCs *In Vitro* and *In Vivo*

(A) Relative expression levels of mature miR-135a in primary NPCs transduced *in vitro* with lentivirus transcribing the immature short-hairpin precursor of miR-135a (sh-miR-135a, i.e., gain of function), or a sponge for miR-135a (sponge miR-135a, i.e., loss of function), or control viruses expressing scrambled RNAs.

(B) Representative micrographs showing immunostaining for Nestin-CFPnuc (green), BrdU-positive cells (red), and GFAP-positive cells (white), and nuclear DNA with DAPI (blue) in the hippocampal SGZ of 6- to 8-week-old *Nestin-CFPnuc* mice, injected with lentiviruses (same used in A), kept 10 days under standard conditions and subjected to three injections of BrdU 24 h before sacrifice.

(C) Representative micrographs showing immunostaining for Nestin-CFPnuc (green), BrdU-positive cells (red) and nuclear DNA with DAPI (blue) in the hippocampal SGZ of 6- to 8-week-old *Nestin-CFPnuc* mice, injected with miR-135a sponge or scrambled-sponge lentivirus, kept 10 days under standard conditions, and subjected to three injections of BrdU 24 h before sacrifice.

(D) Percentage of BrdU and Nestin-CFPnuc double-positive cells over total BrdU+ cells in the SGZ of mice injected with lentiviruses. Data are expressed as means \pm SEM, n = 7 mice per group. One-way ANOVA Bonferroni as *post hoc*. **p < 0.01, ***p < 0.001. Scale bars, 50 μ m (B) and 25 μ m (C).

expected, the proportion of BrdU-positive NPCs in proliferative medium was higher than in quiescence medium (Figures 2A and 2B; p < 0.001) and, consistent with miRNA profiling of running mice (Figure 1), proliferating NPCs had significantly lower levels of miR-135a, miR-190, and miR-203 compared with cells in quiescence (Figure 2C; p < 0.001).

To ascertain whether miR-135a, miR-190, or miR-203 affects adult NPC proliferation, we transfected synthetic miRNA mimics or scrambled control into NPCs *in vitro* and quantified the proliferative marker Ki67 (Bruno and

Darzynkiewicz, 1992). Overexpression of miR-135a, but not miR-203 or miR-190, was sufficient to reduce the proliferation of NPCs (Figures 2D and 2E; p < 0.001). Conversely, inhibition of miR-135a, upon transduction with a virus expressing a sponge (loss of function, see also Figure 3A), led to a significant increase in NPC proliferation (Figures 2D and 2E). These results indicate an anti-proliferative function of miR-135a in adult hippocampal NPCs *in vitro*.

To confirm this result *in vivo*, we transduced lentiviruses expressing either a short-hairpin precursor of miR-135a



(sh-miR-135, gain of function), or a sponge for miR-135a, or scrambled control RNA sequences in NPC cultures (Figure 3A). Expression of miR-135a in NPCs was higher upon transduction with sh-miR-135a and significantly reduced upon transduction with sponge for miR-135a compared with controls (Figure 3A). We injected the miR-135a sponge or a scrambled control lentivirus in the DG of 6- to 8-week-old *Nestin*-CFPnuc mice housed under standard (resting) conditions. Ten days after injection, we found a higher percentage of *Nestin*-CFPnuc⁺ NPCs upon miR-135 inhibition compared with mice injected with the scrambled control using flow cytometry (sponge 1.6%, Figure S2B; control 1.2%, Figure S2A). In another set of experiments (Figures 3, 4, and 5), we administered BrdU (three injections every 2 h) 10 days after virus injection and killed the mice 24 h after the first BrdU administration. We found in both control and miR-135a sponge-injected mice that >90% of the BrdU-positive cells also expressed *Nestin*-CFPnuc (Figures 3B–3D) and glial fibrillary acidic protein (GFAP) (Figure 3B), indicating that the majority of BrdU-positive cells in the SGZ of these mice were *bona fide* NPCs.

Next, we assessed the effect of miR-135a manipulation on NPC proliferation *in vivo*. We injected viruses expressing sh-miR-135, sponge, or scrambled controls into the DG of 8-week-old C57BL/6 mice and placed them in standard cages or in cages equipped with a running wheel for 10 days, followed by BrdU administration (Figure 4A). In resting mice, miR-135a inhibition led to a significant increase in the number of BrdU-positive cells in the SGZ compared with controls (Figures 4B and 4C; $p < 0.01$). In contrast, no significant differences in the number of BrdU-positive cells upon overexpression of miR-135a were observed (Figures 4B and 4C). The latter result could be explained by saturation of the system due to the high expression levels of the endogenous miR-135a in NPCs (Figure 1). Importantly, we found that overexpression of miR-135a prevented running-induced NPC proliferation in the SGZ (Figures 4B and 4C; $p < 0.05$). To corroborate these results, we analyzed the proportion of cells exiting the cell cycle upon miR-135a manipulation in resting and running mice by quantifying BrdU-positive cells that were negative for Ki67 in the SGZ (Figures 4B–4D). Consistent with the antiproliferative function of miR-135a, we found a significant decrease in cell-cycle exit upon injection with the miR-135a sponge in the DG of mice housed under standard conditions (Figure 4D; $p < 0.05$). In contrast, overexpression of miR-135a significantly increased cell-cycle exit in running mice (Figure 4D; $p < 0.01$). These results indicate an antiproliferative function of miR-135a in NPCs and that its downregulation is necessary for the running-induced proliferation in the SGZ of adult mice.

Transient miR-135a Inhibition Stimulates Hippocampal Neurogenesis, but Not Astroglialogenesis *In Vivo*

Next, we asked whether an increased proportion of proliferating NPCs, upon miR-135a inhibition, would also increase neurogenesis (Figure 5). Since constitutive inhibition of miR-135a prevents neuronal differentiation of NPCs (Pons-Espinal et al., 2017), we used synthetic “antagomiRs” to transiently inhibit miR-135a (anti-miR-135a) or scrambled control inhibitors in DG of resting mice and followed the fate of NPCs with BrdU (Figure 5A). As expected, injection of anti-miR-135a dramatically reduced endogenous miR-135a levels compared with control mice (Figure 5B; $p < 0.0001$) and increased NPC proliferation, as indicated by a higher number of BrdU⁺ cells in SGZ of mice (Figures 5C and 5D; $p < 0.0001$). Next, to evaluate the fate of NPCs, we quantified the proportion of cells co-expressing BrdU and the immature neuronal marker doublecortin (DCX) or the postmitotic neuronal marker NeuN in the DG 3 weeks after antagomiRs injection. Interestingly, we found that inhibition of miR-135a increased the proportions of BrdU⁺DCX⁺ (Figures 5E and 5G; $p < 0.0001$) and BrdU⁺NeuN⁺ neurons compared with control mice (Figures 5F and 5H; $p < 0.05$). This result indicated that increased NPC proliferation, upon transient inhibition of miR-135a, leads to enhanced neurogenesis, thus phenocopying running (van Praag et al., 1999). In contrast, miR-135a inhibition did not alter the proportion of BrdU⁺ cells expressing astrocyte markers such as GFAP (Figures S3A and S3B), glutamate transporter GLT-1 (i.e., solute carrier family 1 member 2 [SLC1A2]) (Figures S3C and S3D), or glutamate aspartate transporter (GLAST) (i.e., solute carrier family 1 glial high-affinity glutamate transporter member 3 [SLC1A3]) (Figures S3E and S3F). The latter result is consistent with our previous finding that adult hippocampal NPCs can undergo astroglialogenesis in absence of miRNAs (Pons-Espinal et al., 2017).

Inhibition of miR-135a Re-activates Proliferation in the Hippocampal SGZ of Aged Mice and Stimulates Cell-Cycle Re-entry of Quiescent NPCs

The age-associated reduction in adult neurogenesis has been attributed to exhaustion of the NPC pools and/or to increased NPC quiescence (Encinas et al., 2011; Jaskeliuff et al., 2011; Lugert et al., 2010; Seib et al., 2013). Environmental stimuli have been shown to counteract the age-associated loss of adult neurogenesis in rodents, suggesting that cell-cycle arrest of aged NPCs is reversible, at least to some extent. To verify whether miR-135a inhibition could restore NPC proliferation in the SGZ of aged mice, we injected a sponge for miR-135a in the DG of 8-week-old (young) or 90-week-old (aged) C57BL/6 mice housed under

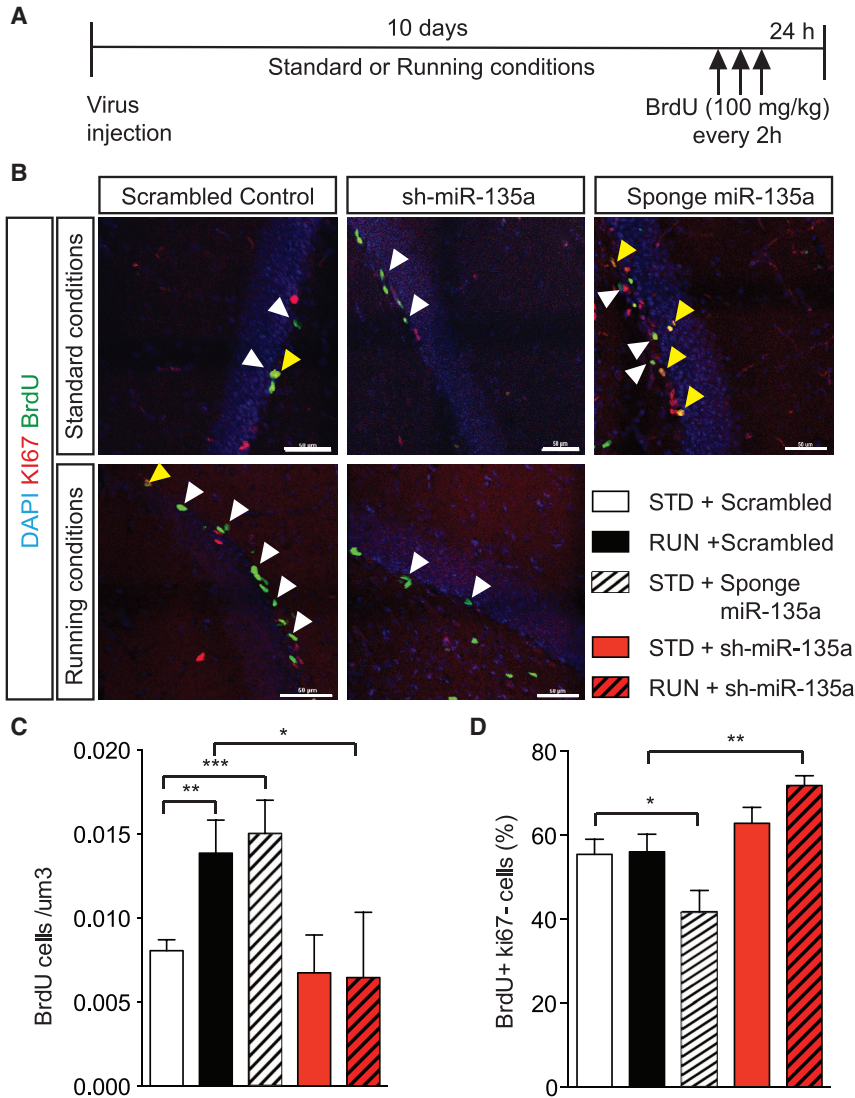


Figure 4. miR-135a Mediates Running-Induced Proliferation in the Hippocampal SGZ *In Vivo*

(A) Schematic representation of the experiment.

(B) Representative micrographs showing BrdU (green), Ki67 (red), or double-positive cells (yellow arrowheads) in the hippocampal SGZ of 6- to 8-week-old C57BL/6 mice, injected with scrambled, sponge miR-135a, or sh-miR-135a virus under standard or running conditions for 10 days and subjected to three injections of BrdU 24 h before sacrifice. White arrowheads, BrdU⁺ Ki67⁻ cells; yellow arrowheads, BrdU⁺ Ki67⁺ cells.

(C) Number of BrdU-positive cells per DG volume (µm³).

(D) Percentage of BrdU⁺Ki67⁻ over total BrdU⁺ cells as a measure of cell-cycle exit.

Data are expressed as means ± SEM, n = 6 mice per group. One-way ANOVA Bonferroni as *post hoc*. *p < 0.05, **p < 0.01, ***p < 0.001. Scale bars, 50 µm.

standard conditions, followed by BrdU administration (as in Figures 3 and 4). Remarkably, inhibition of miR-135a significantly increased the number of BrdU-positive cells in the SGZ of both aged and young mice compared with control mice (Figure 6A). This result indicates that inhibition of miR-135a is sufficient to restore NPC proliferation in the hippocampal SGZ of aged mice, opening the possibility that it might occur through cell-cycle re-entry of quiescent NPC pools. To ascertain this possibility, we over-expressed or inhibited miR-135a in cultured NPCs (Figures 6B–6E). To simulate “aged” adult neurogenesis, we first cultured NPCs in quiescence medium for 72 h, followed by 48 h in fresh proliferative medium (Figure 6B) and measured their capacity to re-enter into proliferative state (Figures 6C–6E) by quantifying BrdU (2 h pulse, Figures 6C and 6D) or Ki67 (Figures 6C–6E). Overexpression of miR-135a impaired NPC proliferation re-entry, as shown

by the lower percentage of BrdU and Ki67 positive NPCs (Figures 6C–6E) compared with control conditions (Figures 6C–6E; p < 0.001, normalized to the short-hairpin control). Interestingly, inhibition of miR-135a stimulated re-entry of NPCs into a proliferative state, as shown by a higher percentage of BrdU and Ki67 positive NPCs compared with the scrambled control (Figures 6C–6E; p < 0.05, normalized to the scrambled sponge). Cell-cycle analysis using propidium iodide and fluorescence-activated cell sorting (FACS) revealed that inhibition of miR-135a significantly increased the proportion of cells in the S phase (10.24% versus 20.63%, p < 0.05) and G2/M phase (9.63% versus 12.61%; Figures S4A and S4B) at the expense of the G1/G0 phase (80.12% versus 66.55%; Figures S4A and S4B; p < 0.01) compared with scrambled control NPCs. Moreover, inhibition of miR-135a in NPCs led to increased mRNA expression of the proliferative markers *Ki67*,

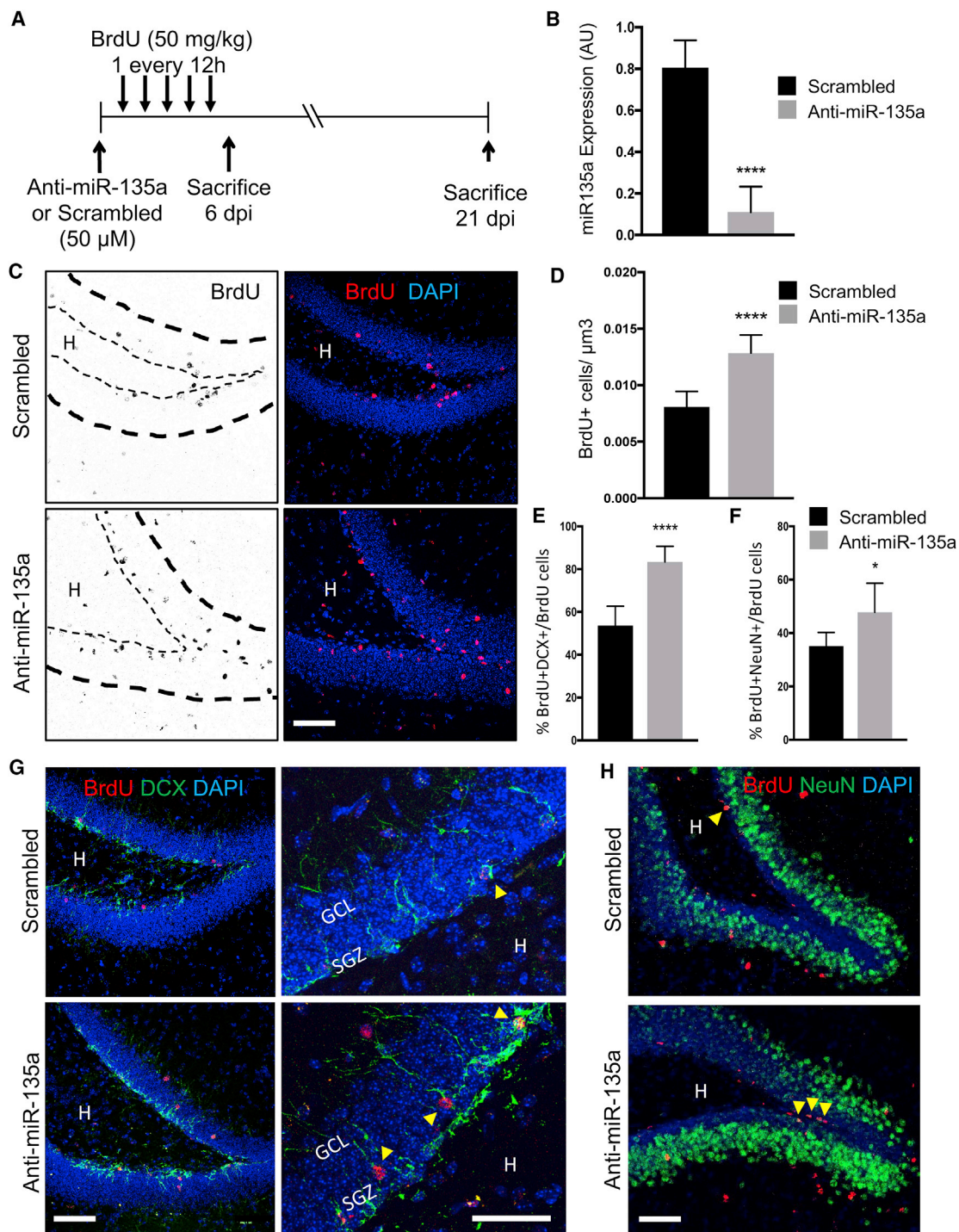


Figure 5. Transient miR-135a Inhibition Stimulates Hippocampal Neurogenesis *In Vivo*

(A) Schematic representation of the experiment.

(B) Relative expression levels of mature miR-135a in hippocampal DG of mice injected with control scrambled or anti-miR-135a 48 h after the injection.

(C and D) (C) Representative micrographs showing BrdU (black or red) cells 6 days after injection of control (scrambled) or anti-miR-135a and (D) the number of BrdU⁺ NPCs per volume (μm^3) in the hippocampal SGZ of 6-week-old C57BL/6 mice.

(legend continued on next page)



Mcm2, and *cyclins A* and *cyclin E* (Figure S4C). Together, these results indicate that inhibition of miR-135a is sufficient to reactivate NPC proliferation in the SGZ of aged mice, suggesting this might occur by stimulating quiescent NPC re-entry into the proliferative state.

Phosphatidylinositol Signaling Proteins Are Modulated by miR-135a in NPCs

To dissect the underlying mechanism of miR-135a in adult hippocampal NPCs, we manipulated its levels *in vitro* and performed shotgun label-free proteomic analysis. Overexpression of miR-135a upregulated 431 proteins (threshold >1.5-fold; Table S2) and downregulated 101 proteins (threshold <0.5-fold; Figure 7A and Table S2); while miR-135a inhibition upregulated 326 proteins (>1.5-fold; Figure 7A and Table S3) and downregulated 109 (<0.5-fold; Table S3). Gene Ontology (GO) analysis with DAVID software (Huang et al., 2009) indicated that the biological functions affected by miR-135a in NPCs were protein transport (GO: 001503; p value sh-miR-135a = 5.59×10^{-6} ; p value miR-135 sponge = 3.29×10^{-4}); vesicle-mediated transport (GO: 0016192; p value sh-miR-135 = 5.34×10^{-5} ; p value miR-135 sponge = 2.10×10^{-3}); transport (GO: 0006810; p value sh-miR-135 = 9.65×10^{-3} ; p value miR-135 sponge = 5.10×10^{-3}), and nervous system development (GO: 0007399; p value sh-miR-135 = 9.79×10^{-3} ; p value miR-135 sponge = 2.81×10^{-2}) (Tables S2 and S3).

miRNAs are mostly post-transcriptional repressors. Hence, to identify potential miR-135a targets, we focused on the downregulated proteins upon miR-135a overexpression and compared them with those upregulated upon miR-135a inhibition in NPCs. Seventeen proteins were consistently modulated by miR-135a levels in both datasets (Figures 7A and 7B). These proteins are involved in an intrinsic apoptotic signaling pathway in response to endoplasmic reticulum stress (GO: 0070059; p = 0.0021, Figure 7C) and a phosphatidylinositol signaling system (mmu04070, p value 0.0249; Figure 7C). The proteins predicted to be involved in these processes were inositol 1,4,5-trisphosphate (IP3) receptor 1 (ITPR1) and BR serine threonine kinase (BRSK2), ITPR1 and inositol polyphosphate-4-phosphatase, type I (INPP4A), respectively (Figure 7C). Interestingly, the human INPP4A transcript is a validated target of miR-135a-5p (DIANA-Tarbase v8.0; Karagkouni et al., 2018) in the brain cortex (Boudreau et al.,

2014) and encodes for an enzyme involved in phosphatidylinositol metabolism. Remarkably, 11 of the 17 hits (64%) are predicted targets of miR-135 (miR-Walk 3.0; Dweep and Gretz, 2015; both miR-135a-5p and miR-135b-5p, collectively defined as miR-135, were considered in the analysis as they share identical seed regions that are conserved in mouse and human) (Figures 7D and 7E), suggesting these proteins could be directly modulated by miR-135. As a control, we repeated the same analysis for the proteins upregulated (>1.5-fold; Table S2) upon miR-135a overexpression and downregulated upon miR-135a inhibition (<0.5-fold; Table S3). However, only 4 (17%) of the 23 proteins consistently modulated by miR-135a in both datasets were predicted targets of either human or mouse miR-135 (not shown), suggesting these proteins are likely indirectly modulated by miR-135.

DISCUSSION

In this study, we identify miR-135a as the first noncoding RNA essential modulator of the brain response to physical exercise. We report that overexpression of miR-135a in the DG prevents running-induced NPC proliferation. On the other hand, miR-135a inhibition stimulates NPC proliferation leading to increased neurogenesis, but not astrogliogenesis, in DG of resting mice. Remarkably, miR-135a inhibition re-activates NPC proliferation in DG of aged mice, likely by stimulating quiescent NPC pools to re-enter the cell cycle.

Several studies reported altered hippocampal miRNA expression in response to physical exercise (Bao et al., 2014; Cosín-Tomás et al., 2014; Hu et al., 2015; Pan-Vazquez et al., 2015) or pathological conditions (Encinas and Fitzsimons, 2017). However, to our knowledge, this is the first study reporting a functional role of an miRNA underlying the exercise-mediated increase in adult neurogenesis. Functions of the two members of the miR-135 family are poorly described in the mammalian CNS. In postmitotic neurons, miR-135 regulates axon growth/regeneration and mediates long-term depression (Hu et al., 2014; van Battum et al., 2017). miR-135a expression is high in the amygdala of stressed mice (Mannironi et al., 2013), and in the mouse raphe nucleus (functionally connected to the hippocampus) it is a key regulator of serotonergic networks and antidepressants action (Issler et al., 2014). However, since

(E and F) Percentage of BrdU⁺DCX⁺ (E), BrdU⁺NeuN⁺ (F) over total BrdU⁺ cells in the hippocampal SGZ of 6-week-old C57BL/6 mice 3 weeks after the injection with scrambled or anti-miR-135a antagonomiRs.

(G and H) Representative micrographs showing staining for BrdU (red), DCX (G, green) or NeuN (H, green); and nuclear DNA with DAPI (blue); arrowheads indicate double-positive cells. H, hilus, GCL, granular cell layer; SGZ, subgranular zone.

Data are expressed as means \pm SEM, n = 7 mice per group. One-way ANOVA Bonferroni as *post hoc*. *p < 0.05, ****p < 0.0001. Scale bars, 50 μ m and 25 μ m (G, high magnification).

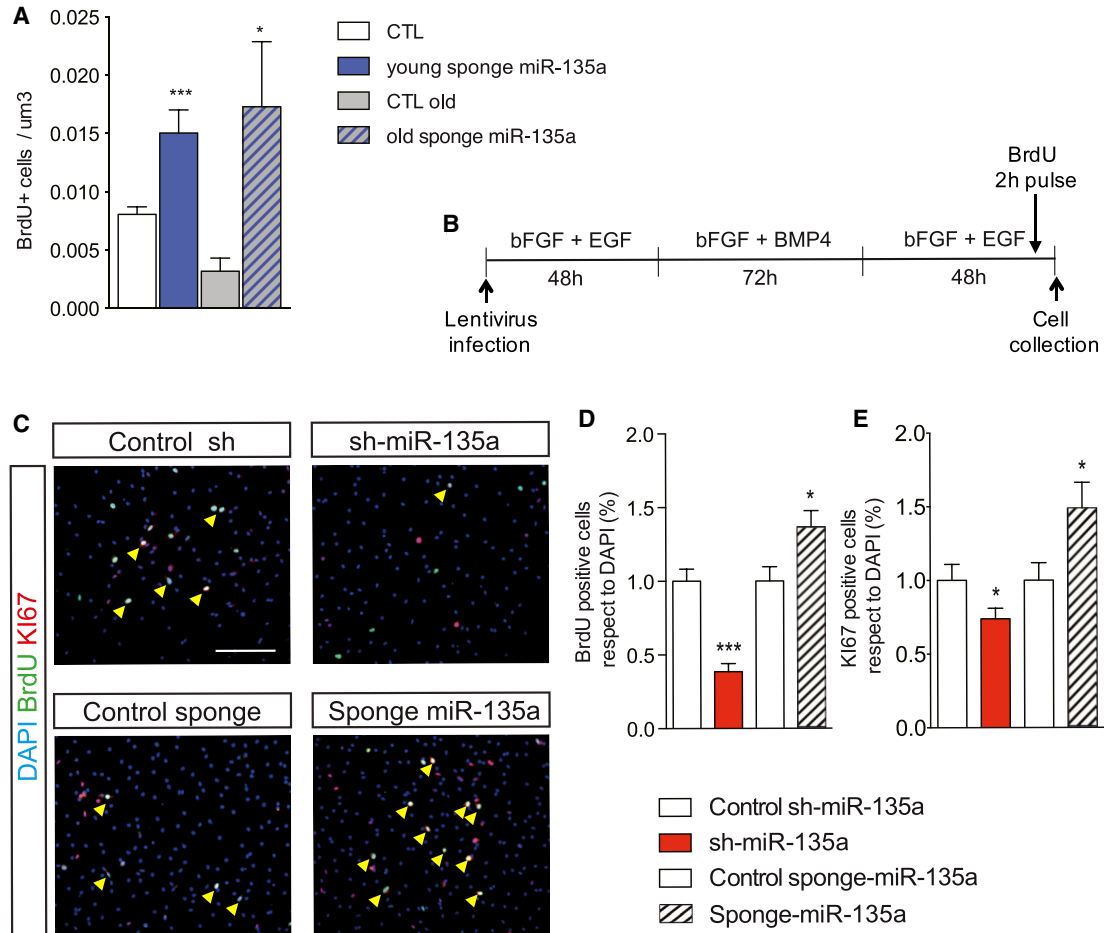


Figure 6. Inhibition of miR-135a Re-activates Proliferation in the Hippocampal SGZ of Aged Mice and Stimulates Cell-Cycle Re-entry of Quiescent NPCs

(A) Number of BrdU⁺ NPCs per DG volume (μm^3) in the hippocampal SGZ of 8-week-old (young) and 90-week-old (aged) C57BL/6 mice, injected with lentiviral sponge for miR-135a (loss of function), housed for 10 days under standard conditions, and subjected to BrdU administration (three injections every 2 h) 24 h before sacrifice.

(B) Schematic representation of the *in vitro* experiment. Primary hippocampal NPCs were allowed to re-enter the cell cycle after 72 h in quiescence medium and fixed 2 h after BrdU administration.

(C) Representative micrographs showing BrdU (green) and Ki67 (red) double-positive cells (yellow, arrowheads) of hippocampal NPCs infected with control sh-scrambled RNA, sh-miR-135a (gain of function), control sponge, or sponge miR-135a lentiviruses.

(D) Percentage of BrdU⁺ cells relative to total cells (DAPI) normalized to controls.

(E) Percentage of Ki67-positive cells relative to total cells (DAPI) normalized to controls.

Data are expressed as means \pm SEM, $n = 3$ independent experiments containing three replicates. One-way ANOVA Bonferroni as *post hoc*. * $p < 0.05$, *** $p < 0.001$. Scale bars, 50 μm .

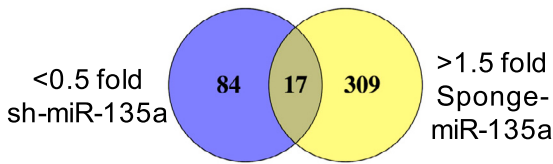
miR-135 association with depression- and anxiety-related phenotypes in patients is very variable (Zurawek et al., 2017), its role in the pathological mechanism of these diseases remains unclear. In the adult mouse hippocampus, miR-135 is rapidly upregulated after prolonged kainic acid-induced seizures (Schouten et al., 2015). Moreover, we recently found that miR-135a is one of the 11 miRNAs required and sufficient to sustain the neurogenic lineage fate of NPCs (Pons-Espinal et al., 2017). Hence, miR-135 is

required to regulate multiple aspects of adult hippocampal neurogenesis, suggesting that further studies on miR-135 in the brain response to physiological and pathological conditions are warranted.

Physical exercise is a potent trigger of adult hippocampal neurogenesis in both young and aged mice, but cellular and molecular mechanisms underlying this phenomenon remain controversial. Cellular mechanisms include recruitment of quiescent neural stem cells, acceleration of the cell



A



B

ID protein (UniProtKB)	ID ENSEMBL	FULL NAME	Predicted Target?
ITPR1	ITPR1	Inositol 1,4,5-Trisphosphate Receptor Type 1	YES
RUFY3	RUFY3	RUN And FYVE Domain Containing 3	YES
MRCKB	CDC42BPB	CDC42 Binding Protein Kinase Beta	YES
ASTN1	ASTN1	Astrotactin 1	YES
F6V2U0	Inpp4a-213	Inositol Polyphosphate-4-Phosphatase Type I A	YES
CREL2	CRELD2	Cysteine-rich with EGF-like domain protein 2	NO TARGET
G3UWV4	BRSK2	BR Serine/threonine-protein kinase BRSK2	YES
EFR3B	EFR3B	EFR3 Homolog B	NO TARGET
EPDR1	EPDR1	Ependymin Related 1	NO TARGET
Q91V77	S100A1	S100 Calcium Binding Protein A1	NO TARGET
NOP9	NOP9	NOP9 Nucleolar Protein (Pumilio Domain-Containing Protein C14orf21)	YES
D3YTR6	SPNS1	Spinster homolog 1 (Putative sphingolipid transporter 1)	YES
TMED1	TMED1	Transmembrane P24 Trafficking Protein 1	NO TARGET
DYN1	DNM1	Dynamain 1	YES
CCD51	CCD51	Coiled-Coil Domain Containing 51	YES
Q9D1F0	RTL8B	CAAX box 1 homolog A	NO TARGET
HPF1	HPF1	Histone PARylation Factor 1	Yes

C

GO Biological process TERM: 0070059 ~ intrinsic apoptotic signaling pathway response to E.R. stress	P value: 0,02169	PROTEINS INVOLVED ON THE BIOLOGICAL PROCESS: Brsk2 ; Itpr1
mmu04070:Phosphatidylinositol signaling system	P value: 0,02497	PROTEINS INVOLVED ON THE KEGG PATHWAY: Itpr1; Inpp4a

E

miRNA-id	Ensembl-id	Gene	Start	End	Binding length	Longest pairings	Location
mmu-miR-135a-5p	ENSMUST00000078200	Brsk2	3492	3507	15	14	3UTR
	ENSMUST00000075528		3857	3872	15	14	
	ENSMUST00000018971		3397	3412	15	14	
mmu-miR-135b-5p	ENSMUST00000019441	Nop9	3273	3292	19	13	3UTR
	ENST00000074304	INPP4A	4399	4418	19	8	
ENST00000409016	4282		4301	19	8		
ENST00000409851	4384		4403	19	8		
hsa-miR-135a-5p	ENST00000357086	ITPR1	8002	8032	15	13	CDS
hsa-miR-135b-5p	ENST00000357086		7995	8032	15	13	
hsa-miR-135a-5p	ENST00000302640		8101	8131	15	13	
hsa-miR-135b-5p	ENST00000302640	ITPR1	8094	8131	15	13	CDS
hsa-miR-135a-5p	ENST00000354582		8146	8176	15	13	
hsa-miR-135b-5p	ENST00000354582		8139	8176	15	13	
hsa-miR-135b-5p	ENST00000417478	RUFY3	652	676	24	8	CDS
	ENST00000381006		1204	1228	24	8	CDS
	ENST00000226328		4015	4058	43	11	3UTR
	ENST00000226328		1204	1228	24	8	CDS
hsa-miR-135a-5p	ENST00000502653	CDC42BPB	596	620	24	8	CDS
hsa-miR-135b-5p	ENST00000361246		3509	3537	28	10	CDS
hsa-miR-135b-5p	ENST00000361833	ASTN1	6434	6457	23	10	3UTR
	ENST00000531197	BRSK2	3223	3242	19	13	3UTR
	ENST00000528841		3646	3665	19	13	
ENST00000308219	3176		3195	19	13		
hsa-miR-135b-5p	ENST00000528710	BRSK2	3210	3229	19	13	3UTR
	ENST00000382179		3603	3622	19	13	
	ENST00000267425		4611	4630	19	12	
hsa-miR-135b-5p	ENST00000396802	NOP9	4445	4464	19	12	3UTR
	ENST00000341179	DNM1	806	833	27	7	CDS
ENST00000372923	806		833	27	7		
ENST00000475805	806		833	27	7		
hsa-miR-135b-5p	ENST00000393594	DNM1	806	833	27	7	CDS
	ENST00000486160		806	833	27	7	
	ENST00000627543		806	833	27	7	
hsa-miR-135a-5p	ENST00000628346	SPNS1	806	833	27	7	CDS
	ENST00000566059		827	856	18	9	
	ENST00000566059		827	856	18	9	
hsa-miR-135b-5p	ENST00000566059	SPNS1	625	645	20	9	CDS
hsa-miR-135a-5p	ENST00000565975		807	836	18	9	
hsa-miR-135b-5p	ENST00000565975		788	836	18	9	
hsa-miR-135b-5p	ENST00000565975	SPNS1	620	640	20	9	CDS
hsa-miR-135a-5p	ENST00000311008		1041	1070	18	9	
hsa-miR-135b-5p	ENST00000311008		1022	1070	18	9	
hsa-miR-135b-5p	ENST00000311008	SPNS1	854	874	20	9	CDS
hsa-miR-135a-5p	ENST00000334536		1041	1070	18	9	
hsa-miR-135a-5p	ENST00000352260		975	1004	18	9	
hsa-miR-135b-5p	ENST00000352260	SPNS1	956	1004	18	9	CDS
hsa-miR-135b-5p	ENST00000352260		788	808	20	9	
hsa-miR-135a-5p	ENST00000323081		954	983	18	9	
hsa-miR-135b-5p	ENST00000323081	HPF1	935	983	18	9	CDS
hsa-miR-135b-5p	ENST00000323081		767	787	20	9	
hsa-miR-135b-5p	ENST00000393381		234	271	37	11	
hsa-miR-135b-5p	ENST00000442740	CCDC51	332	386	24	12	5UTR
hsa-miR-135b-5p	ENST00000395694		933	955	22	9	CDS

D

Alignment miR-135a/b-5-p: mmu (Mouse); Hsa (Human)	
mmu-miR-135b-5p	5'-UAUGGCUUUU CAU UCCUAUGUGA-3'
hsa-miR-135b-5p	5'-UAUGGCUUUU CAU UCCUAUGUGA-3'
mmu-miR-135a-5p	5'-UAUGGCUUUU UAU UCCUAUGUGA-3'
hsa-miR-135a-5p	5'-UAUGGCUUUU UAU UCCUAUGUGA-3'

Figure 7. Phosphatidylinositol Signaling Proteins Are Modulated by miR-135a in NPCs

(A and B) Venn diagram indicating the number of downregulated proteins (purple, <math><0.5</math>-fold) upon overexpression of miR-135a (sh-miR-135a), or upregulated proteins (yellow, >1.5-fold) upon inhibition of miR-135a (Sponge-miR-135a), and the 17 differently expressed proteins (table in B) found in both datasets, in cultured primary hippocampal NPCs.

(C) *In silico* GO analysis and KEGG pathway analysis.

(D) Alignment of mouse and human miR-135a-5p and miR-135b-5p.

(E) Predicted targets of miR135 according to MiRWalk. Position and length of predicted target sites of miR-135a-5p and miR-135b-5p are shown for each transcript (Ensembl ID).

cycle of NPCs, increased number of cell divisions, and reduction of cell death (Overall et al., 2016). At the molecular level, physical exercise has been shown to increase

levels of growth factors BDNF, IGF, FGF-2, and VEGF, leading to the activation of MAPK/ERK and PI3K-Akt signaling pathways (Cotman et al., 2007). We report that INPP4A, a



key enzyme for phosphatidylinositol metabolism and known target of miR-135 in the cortex (Boudreau et al., 2014), is one of the top proteins modulated by miR-135 in NPCs. ITPR1, another differentially expressed protein identified in our analysis, is also a key player in IP3 signaling. Hence, phosphatidylinositol signaling could represent a prominent constraint to NPC proliferative potential. This hypothesis is consistent with previous studies indicating that the PI3K-Akt signaling pathway is activated by exercise in rodents (Bruel-Jungerman et al., 2009; Chen and Russo-Neustadt, 2005). However, while these studies concluded that the PI3K-Akt pathway primarily mediates the effect of exercise on the survival of newly generated DG neurons and the associated increase in synaptic plasticity, our results suggest that miR-135/phosphatidylinositol signaling could mediate exercise-induced proliferation of NPCs. Together, this evidence opens the possibility that the miR-135-IP3-axis might represent a novel target of therapeutic intervention to stimulate adult neurogenesis.

One unanswered question arising from our study is how running decreases miR-135 levels in adult NPCs. miR-135 is a tumor suppressor (Cheng et al., 2017; Xu et al., 2016), which is downregulated in several cancers (Guo et al., 2018; Mao et al., 2015; Pei et al., 2015; Wu et al., 2012; Zubieta et al., 2017). A Wnt/miR-135a auto-regulatory loop has been identified in brain development, which could modulate differentiation of forebrain (Caronia-Brown et al., 2016) and dopaminergic (Anderegg et al., 2013; De Gregorio et al., 2018) neurons. Moreover, Wnt/TGF β /BMP pathways are known to influence long-term maintenance of NPC pools in the adult hippocampus, age-associated cognitive decline, and brain dysfunctions (Inestrosa and Arenas, 2010; Urban and Guillemot, 2014). This evidence provides possible mechanisms to explain the rescue of proliferation in the hippocampal stem cell niche of aged mice upon miR-135 downregulation.

In summary, we propose that the therapeutic exploitation of miR-135 might offer intriguing perspectives to delay or prevent pathological brain aging.

EXPERIMENTAL PROCEDURES

Animal Model

Mice (C57BL/6J, Jackson Lab no. 000664; Td-Tomato^{fllox/wt} knockin reporter mice, Jackson Lab no. 007908; Madisen et al., 2010; Nestin-CFPnuc, Encinas et al., 2006) were housed under standard laboratory conditions at Istituto Italiano di Tecnologia (IIT), the Center for Regenerative Therapies Dresden (CRTD), or the Medizinische-Theoretisches Zentrum (MTZ) Dresden. Experiments were approved by the Italian and German authorities (permit nos. 056/2013, 214/2015-PR, and 24-9168.11-1/2013-15) and conducted in accordance with the Guide for the Care and Use of Laboratory Animals of the European Community Direc-

tives. Mice were maintained under a 12 h light/dark cycle with food and water *ad libitum*.

NPC Culture

Hippocampal NPCs were prepared as previously published (Babu et al., 2011) from ten 6-week-old C57BL/6J mice and cultured as previously described (Pons-Espinal et al., 2017). For quiescence, 1.2×10^4 cells/cm² were plated into normal proliferation medium; after 16 h, quiescence medium (50 ng/mL BMP4 [R&D Systems] and 20 ng/mL bFGF; Martynoga et al., 2013) was added.

Running

Nine-week-old Nestin-CFPnuc mice or WT C57BL/6J were double housed under standard conditions or in cages equipped with a running wheel (TSE System, animal facility of CRTD; or ENV-044 [Med Associates], Animal facility of IIT) for 10 days before sacrifice. Twenty-four hours before sacrifice, mice received one administration of 50 mg/kg BrdU (B9285, Sigma).

miRNA Manipulation

Mimics and antagomiRs used are listed in Supplemental Experimental Procedures. Scrambled miRNA mimics (50 nM; QIAGEN) or miRNA antagomiRs (150 nM; QIAGEN) were nucleofected (Amaxa) in proliferating or quiescent NPC cultures. Then, 48 h after nucleofection, 10 μ M BrdU was added to the medium for 2 h, followed by fixation (4% PFA) or RNA/protein extraction. Virus and synthetic oligos were stereotaxically injected in the hippocampus (coordinates: -2.0 A/P, ± 1.6 M/L, and -1.9 to -2.1 D/V relative to bregma [mm]) as previously described (Pons-Espinal et al., 2017). Codes for viruses and oligos are listed in Supplemental Experimental Procedures. After virus injection, mice received three BrdU intraperitoneal injections per day (100 mg/kg, every 2 h) and sacrificed 24 h later. After injection of oligos, mice received two BrdU intraperitoneal injections per day (50 mg/kg) for 5 days and sacrificed 2 h (6 days post injection of oligos) or 2 weeks after the last BrdU injection (21 days post injection of oligos).

Immunofluorescence and Cell Quantification

Immunofluorescence staining on brain slices (40 μ m) was performed in one of every six sections of the hippocampus. A list of primary antibodies and the detailed protocol is provided in the Supplemental Experimental Procedures. Confocal stack images of brain slices were obtained with the Confocal A1 Nikon Inverted SFC with 40 \times objective and the Zeiss Spinning Disc with a 20 \times objective. Cell quantification and analysis were performed using NIS-Elements software (Nikon) and ZenBlue (Zeiss). Immunofluorescence on cell cultures was performed as previously described (Pons-Espinal et al., 2017). Images were obtained using a Nikon Eclipse microscope at 20 \times or 40 \times magnification, and quantification was performed using a cell-counter plugin in Fiji (Fiji is just ImageJ; Schindelin et al., 2012).

FACS and RNA Analysis

For RNA extraction and cDNA preparation, 6–10 Nestin-CFPnuc mice per condition were euthanized at the indicated times. Cells were dissociated with the Neural Tissue Dissociation Kit P (Miltenyi),



FACS sorted, and immediately processed for RNA extraction (Walker et al., 2016). Total RNA was extracted with QIAzol (QIAGEN), RNA was purified with an RNeasy Kit, or miRNeasy Kit (QIAGEN) following the manufacturer's instructions. Quantification of RNA was performed as in Pons-Espinal et al. (2017).

In Situ Hybridization

In situ hybridization was performed as previously published (De Pietri Tonelli et al., 2014) with minor modifications. Brain slices (18–20 μ m) were permeabilized and post-fixed in 4% PFA. Slides were blocked with 0.25% acetic anhydride (Sigma), and a pre-hybridization solution was added, followed by incubation with a hybridization solution containing 160 nM (miR-135, -190, -203) or 100 nM (miR-9) of the DIG-labeled LNA probe (Exiqon) overnight. The anti-DIG antibody (Roche; 1:2000) was incubated overnight at 4°C. For development of the color reactions, two different alkaline phosphatase substrates were used: NBT/BCIP (Roche) or Fast Red TR/Naphthol AS-MX solution (Sigma), following the manufacturers' instructions. Sections were mounted and imaged using conventional bright-field microscopy or a confocal microscope with the Cy-3 filter.

Proteomics

NPCs (three independent experiments) were lysed with RIPA buffer, and 50 μ g of proteins was collected from all the samples and processed as previously described (Braccia et al., 2018). Protein pools were processed for liquid chromatography-tandem mass spectrometry analysis.

Statistical Analysis

Data are presented as means \pm SEM and were analyzed using Prism 6 (GraphPad). Statistical details of the experiments can be found in the Results and figure legends. Statistical significance was assessed with a two-tailed unpaired t test for two experimental groups. For experiments with three or more groups, one-way ANOVA with Bonferroni's multiple comparison test *post hoc* was used. Mean differences were considered to be statistically significant when $p < 0.05$.

ACCESSION NUMBERS

All the RAW data files used for protein quantification acquired for the present work are freely available through the ProteomeExchange database (Vizcaino et al., 2014; Deutsch et al., 2017) with identifier ProteomeXchange: PXD009845.

SUPPLEMENTAL INFORMATION

Supplemental Information can be found online at <https://doi.org/10.1016/j.stemcr.2019.04.020>.

AUTHOR CONTRIBUTIONS

M.P.E., C.G., and D.D.P.T. co-designed the experiments. M.P.E. and C.G. performed most of the experiments, analyzed the data, prepared the figures, and drafted the manuscript. T.L.W. and A.P. carried out experiments and analyzed the data of Figures 1A–1D and S2 under the supervision of K.F. and G.K. M.J.M. performed quan-

tification and analysis of miRNA expression (Figures 1E and S1 and Table S1) under the supervision of F.N. C.B. prepared the SWATH library and performed mass spectrometry under the supervision of A.A. D.D.P.T. conceived and coordinated the project and wrote the manuscript. All authors edited and approved the final version of the manuscript.

ACKNOWLEDGMENTS

We are grateful to Dr. G. Enikolopov (Stony Brook University, New York) for kindly providing the *Nestin*-CFPnuc mouse line. We thank R. Pelizzoli for generation of the viruses and help with NPC cultures and western blot, the technical staff of IIT (M. Pesce, imaging; E. Albanesi, FACS facility) and of DZNE (N Rund, FACS; and P. Oloth, histology of Figures 1B and 1C) for excellent assistance. Images for Figure 1D were acquired and processed using equipment of the DZNE-Imaging facility. We thank the staff of IIT Animal Facility and M. Morini for excellent assistance with animal experiments. This study was supported by intramural funds of Fondazione Istituto Italiano di Tecnologia (IIT) and partly by Fondazione Cariplo grant no. 2015-0590 to D.D.P.T. and F.N. and AIRC IG 2017 ID 20106 to D.D.P.T.

Received: June 5, 2018

Revised: April 23, 2019

Accepted: April 24, 2019

Published: May 23, 2019

REFERENCES

- Anderegg, A., Lin, H.P., Chen, J.A., Caronia-Brown, G., Cherepanova, N., Yun, B., Joksimovic, M., Rock, J., Harfe, B.D., Johnson, R., et al. (2013). An *Lmx1b*-miR135a2 regulatory circuit modulates *Wnt1/Wnt* signaling and determines the size of the midbrain dopaminergic progenitor pool. *PLoS Genet.* 9, e1003973.
- Babu, H., Claasen, J.H., Kannan, S., Rünker, A.E., Palmer, T., and Kempermann, G. (2011). A protocol for isolation and enriched monolayer cultivation of neural precursor cells from mouse dentate gyrus. *Front. Neurosci.* 5, 89.
- Bao, T.H., Miao, W., Han, J.H., Yin, M., Yan, Y., Wang, W.W., and Zhu, Y.H. (2014). Spontaneous running wheel improves cognitive functions of mouse associated with miRNA expressional alteration in hippocampus following traumatic brain injury. *J. Mol. Neurosci.* 54, 622–629.
- Barca-Mayo, O., and De Pietri Tonelli, D. (2014). Convergent microRNA actions coordinate neocortical development. *Cell. Mol. Life Sci.* 71, 2975–2995.
- Bond, A.M., Ming, G.L., and Song, H. (2015). Adult mammalian neural stem cells and neurogenesis: five decades later. *Cell Stem Cell* 17, 385–395.
- Boudreau, R.L., Jiang, P., Gilmore, B.L., Spengler, R.M., Tirabassi, R., Nelson, J.A., Ross, C.A., Xing, Y., and Davidson, B.L. (2014). Transcriptome-wide discovery of microRNA binding sites in Human Brain. *Neuron* 81, 294–305.
- Braccia, C., Espinal, M.P., Pini, M., De Pietri Tonelli, D., and Armirotti, A. (2018). A new SWATH ion library for mouse adult hippocampal neural stem cells. *Data Brief* 18, 1–8.



- Bruel-Jungerman, E., Veyrac, A., Dufour, F., Horwood, J., Laroche, S., and Davis, S. (2009). Inhibition of PI3K-Akt signaling blocks exercise-mediated enhancement of adult neurogenesis and synaptic plasticity in the dentate gyrus. *PLoS One* 4, e7901.
- Bruno, S., and Darzynkiewicz, Z. (1992). Cell cycle dependent expression and stability of the nuclear protein detected by Ki-67 antibody in HL-60 cells. *Cell Prolif.* 25, 31–40.
- Caronia-Brown, G., Anderegg, A., and Awatramani, R. (2016). Expression and functional analysis of the Wnt/beta-catenin induced mir-135a-2 locus in embryonic forebrain development. *Neural Dev.* 11, 9.
- Chen, M.J., and Russo-Neustadt, A.A. (2005). Exercise activates the phosphatidylinositol 3-kinase pathway. *Mol. Brain Res.* 135, 181–193.
- Cheng, Z., Liu, F., Zhang, H., Li, X., Li, Y., Li, J., Liu, F., Cao, Y., Cao, L., and Li, F. (2017). miR-135a inhibits tumor metastasis and angiogenesis by targeting FAK pathway. *Oncotarget* 8, 31153–31168.
- Cosín-Tomás, M., Alvarez-López, M.J., Sanchez-Roige, S., Lalanza, J.F., Bayod, S., Sanfeliu, C., Pallàs, M., Escorihuela, R.M., and Kaliman, P. (2014). Epigenetic alterations in hippocampus of SAMP8 senescent mice and modulation by voluntary physical exercise. *Front. Aging Neurosci.* 6, 51.
- Cotman, C.W., Berchtold, N.C., and Christie, L.A. (2007). Exercise builds brain health: key roles of growth factor cascades and inflammation. *Trends Neurosci.* 30, 464–472.
- De Gregorio, R., Pulcrano, S., De Sanctis, C., Volpicelli, F., Guatteo, E., von Oerthel, L., Latagliata, E.C., Esposito, R., Piscitelli, R.M., Perrone-Capano, C., et al. (2018). miR-34b/c regulates Wnt1 and enhances mesencephalic dopaminergic neuron differentiation. *Stem Cell Reports* 10, 1237–1250.
- Dennis, C.V., Suh, L.S., Rodriguez, M.L., Kril, J.J., and Sutherland, G.T. (2016). Human adult neurogenesis across the ages: an immunohistochemical study. *Neuropathol. Appl. Neurobiol.* 42, 621–638.
- De Pietri Tonelli, D., Clovis, Y.M., and Huttner, W.B. (2014). Detection and monitoring of microRNA expression in developing mouse brain and fixed brain cryosections. *Methods Mol. Biol.* 1092, 31–42.
- Deutsch, E.W., Csordas, A., Sun, Z., Jarnuczak, A., Perez-Riverol, Y., Ternent, T., Campbell, D.S., Bernal-Llinares, M., Okuda, S., Kawano, S., et al. (2017). The ProteomeXchange consortium in 2017: supporting the cultural change in proteomics public data deposition. *Nucleic Acids Res.* 45, D1100–D1106.
- Dweep, H., and Gretz, N. (2015). MiRWalk2.0: a comprehensive atlas of microRNA-target interactions. *Nat. Methods* 12, 697.
- Encinas, J.M., Vaahtokari, A., and Enikolopov, G. (2006). Fluoxetine targets early progenitor cells in the adult brain. *Proc. Natl. Acad. Sci. U S A* 103, 8233–8238.
- Encinas, J.M., Michurina, T.V., Peunova, N., Park, J.H., Tordo, J., Peterson, D.A., Fishell, G., Koulakov, A., and Enikolopov, G. (2011). Division-coupled astrocytic differentiation and age-related depletion of neural stem cells in the adult hippocampus. *Cell Stem Cell* 8, 566–579.
- Encinas, J.M., and Fitzsimons, C.P. (2017). Gene regulation in adult neural stem cells. Current challenges and possible applications. *Adv. Drug Deliv. Rev.* 120, 118–132.
- Eriksson, P.S., Perfilieva, E., Björk-Eriksson, T., Alborn, A.-M., Nordborg, C., Peterson, D.A., and Gage, F.H. (1998). Neurogenesis in the adult human hippocampus. *Nat. Med.* 4, 1313–1317.
- Farioli-Vecchioli, S., Mattera, A., Micheli, L., Ceccarelli, M., Leonardi, L., Saraulli, D., Costanzi, M., Cestari, V., Rouault, J.P., and Tirone, F. (2014). Running rescues defective adult neurogenesis by shortening the length of the cell cycle of neural stem and progenitor cells. *Stem Cells* 32, 1968–1982.
- Fischer, T.J., Walker, T.L., Overall, R.W., Brandt, M.D., and Kempermann, G. (2014). Acute effects of wheel running on adult hippocampal precursor cells in mice are not caused by changes in cell cycle length or S phase length. *Front. Neurosci.* 8, 314.
- Guo, L., Ding, G., Xu, W., Ge, H., Jiang, Y., Chen, X., and Lu, Y. (2018). MiR-135a-5p represses proliferation of HNSCC by targeting HOXA10. *Cancer Biol. Ther.* 19, 1–28.
- Hu, T., Zhou, F.J., Chang, Y.F., Li, Y.S., Liu, G.C., Hong, Y., Chen, H.L., Xiyang, Y.B., and Bao, T.H. (2015). miR21 is associated with the cognitive improvement following voluntary running wheel exercise in TBI mice. *J. Mol. Neurosci.* 57, 114–122.
- Hu, Z., Yu, D., Gu, Q.H., Yang, Y., Tu, K., Zhu, J., and Li, Z. (2014). MiR-191 and miR-135 are required for long-lasting spine remodeling associated with synaptic long-term depression. *Nat. Commun.* 5, 3263.
- Huang, D.W., Sherman, B.T., and Lempicki, R.A. (2009). Systematic and integrative analysis of large gene lists using DAVID bioinformatics resources. *Nat. Protoc.* 4, 44–57.
- Inestrosa, N.C., and Arenas, E. (2010). Emerging roles of Wnts in the adult nervous system. *Nat. Rev. Neurosci.* 11, 77–86.
- Issler, O., Haramati, S., Paul, E.D., Maeno, H., Navon, I., Zwang, R., Gil, S., Mayberg, H.S., Dunlop, B.W., Menke, A., et al. (2014). MicroRNA 135 is essential for chronic stress resiliency, antidepressant efficacy, and intact serotonergic activity. *Neuron* 83, 344–360.
- Jaskelioff, M., Muller, F.L., Paik, J.H., Thomas, E., Jiang, S., Adams, A.C., Sahin, E., Kost-Alimova, M., Protopopov, A., Cadiñanos, J., et al. (2011). Telomerase reactivation reverses tissue degeneration in aged telomerase-deficient mice. *Nature* 469, 102–107.
- Karagkouni, D., Paraskevopoulou, M.D., Chatzopoulos, S., Vlachos, I.S., Tastsoglou, S., Kanellos, I., Papadimitriou, D., Kavakiotis, I., Manioui, S., Skoufos, G., et al. (2018). DIANA-TarBase v8: a decade-long collection of experimentally supported miRNA-gene interactions. *Nucleic Acids Res.* 46, D239–D245.
- Kempermann, G., Kuhn, H.G., and Gage, F.H. (1998). Experience-induced neurogenesis in the senescent dentate gyrus. *J. Neurosci.* 18, 3206–3212.
- Kempermann, G. (2011). Seven principles in the regulation of adult neurogenesis. *Eur. J. Neurosci.* 33, 1018–1024.
- Kempermann, G., Gage, F.H., Aigner, L., Song, H., Curtis, M.A., Thuret, S., Kuhn, H.G., Jessberger, S., Frankland, P.W., Cameron, H.A., et al. (2018). Human adult neurogenesis: evidence and remaining questions. *Cell Stem Cell* 23, 25–30.
- Kempermann, G., Gast, D., and Gage, F.H. (2002). Neuroplasticity in old age: sustained fivefold induction of hippocampal neurogenesis



- by long-term environmental enrichment. *Ann. Neurol.* 52, 135–143.
- Knoth, R., Singec, I., Ditter, M., Pantazis, G., Capetian, P., Meyer, R.P., Horvat, V., Volk, B., and Kempermann, G. (2010). Murine features of neurogenesis in the human hippocampus across the lifespan from 0 to 100 years. *PLoS One* 5, e8809.
- Kronenberg, G., Bick-Sander, A., Bunk, E., Wolf, C., Ehninger, D., and Kempermann, G. (2006). Physical exercise prevents age-related decline in precursor cell activity in the mouse dentate gyrus. *Neurobiol. Aging* 27, 1505–1513.
- Kronenberg, G., Reuter, K., Steiner, B., Brandt, M.D., Jessberger, S., Yamaguchi, M., and Kempermann, G. (2003). Subpopulations of proliferating cells of the adult hippocampus respond differently to physiologic neurogenic stimuli. *J. Comp. Neurol.* 467, 455–463.
- Lugert, S., Basak, O., Knuckles, P., Haussler, U., Fabel, K., Götz, M., Haas, C.A., Kempermann, G., Taylor, V., and Giachino, C. (2010). Quiescent and active hippocampal neural stem cells with distinct morphologies respond selectively to physiological and pathological stimuli and aging. *Cell Stem Cell* 6, 445–456.
- Madisen, L., Zwingman, T.A., Sunkin, S.M., Oh, S.W., Zariwala, H.A., Gu, H., Ng, L.L., Palmiter, R.D., Hawrylycz, M.J., Jones, A.R., et al. (2010). A robust and high-throughput Cre reporting and characterization system for the whole mouse brain. *Nat. Neurosci.* 13, 133–140.
- Mannironi, C., Camon, J., De Vito, F., Biundo, A., De Stefano, M.E., Persiconi, I., Bozzoni, I., Fragapane, P., Mele, A., and Presutti, C. (2013). Acute stress alters amygdala microRNA miR-135a and miR-124 expression: inferences for corticosteroid dependent stress response. *PLoS One* 8, e73385.
- Mao, X.P., Zhang, L.S., Huang, B., Zhou, S.Y., Liao, J., Chen, L.W., Qiu, S.P., and Chen, J.X. (2015). Mir-135a enhances cellular proliferation through post-transcriptionally regulating PHLPP2 and FOXO1 in human bladder cancer. *J. Transl. Med.* 13, 86.
- Martynoga, B., Mateo, J.L., Zhou, B., Andersen, J., Achimastou, A., Urbán, N., van den Berg, D., Georgopoulou, D., Hadjur, S., Wittbrodt, J., et al. (2013). Epigenomic enhancer annotation reveals a key role for NFIX in neural stem cell quiescence. *Genes Dev.* 27, 1769–1786.
- Mathews, K.J., Allen, K.M., Boerrigter, D., Ball, H., Shannon Weickert, C., and Double, K.L. (2017). Evidence for reduced neurogenesis in the aging human hippocampus despite stable stem cell markers. *Aging Cell* 16, 1195–1199.
- Overall, R.W., Walker, T.L., Fischer, T.J., Brandt, M.D., and Kempermann, G. (2016). Different mechanisms must be considered to explain the increase in hippocampal neural precursor cell proliferation by physical activity. *Front. Neurosci.* 10, 362.
- Overall, R.W., Walker, T.L., Leiter, O., Lenke, S., Ruhwald, S., and Kempermann, G. (2013). Delayed and transient increase of adult hippocampal neurogenesis by physical exercise in DBA/2 mice. *PLoS One* 8, e83797.
- Pan-Vazquez, A., Rye, N., Ameri, M., McSparron, B., Smallwood, G., Bickerdyke, J., Rathbone, A., Dajas-Bailador, F., and Toledo-Rodriguez, M. (2015). Impact of voluntary exercise and housing conditions on hippocampal glucocorticoid receptor, miR-124 and anxiety. *Mol. Brain* 8, 40.
- Pei, H., Jin, Z., Chen, S., Sun, X., Yu, J., and Guo, W. (2015). MiR-135b promotes proliferation and invasion of osteosarcoma cells via targeting FOXO1. *Mol. Cell. Biochem.* 400, 245–252.
- Pons-Espinal, M., de Luca, E., Marzi, M.J., Beckervordersandforth, R., Armirotti, A., Nicassio, F., Fabel, K., Kempermann, G., and De Pietri Tonelli, D. (2017). Synergic functions of miRNAs determine neuronal fate of adult neural stem cells. *Stem Cell Reports* 8, 1046–1061.
- Schindelin, J., Arganda-Carreras, I., Frise, E., Kaynig, V., Longair, M., Pietzsch, T., Preibisch, S., Rueden, C., Saalfeld, S., Schmid, B., et al. (2012). Fiji: an open-source platform for biological-image analysis. *Nat. Methods* 9, 676–682.
- Schouten, M., Fratantoni, S.A., Hubens, C.J., Piersma, S.R., Pham, T.V., Bielefeld, P., Voskuyl, R.A., Lucassen, P.J., Jimenez, C.R., and Fitzsimons, C.P. (2015). MicroRNA-124 and -137 cooperativity controls caspase-3 activity through BCL2L13 in hippocampal neural stem cells. *Sci. Rep.* 5, 12448.
- Seib, D.R.M., Corsini, N.S., Ellwanger, K., Plaas, C., Mateos, A., Pitzer, C., Niehrs, C., Celikel, T., and Martin-Villalba, A. (2013). Loss of dickkopf-1 restores neurogenesis in old age and counteracts cognitive decline. *Cell Stem Cell* 12, 204–214.
- Selbach, M., Schwanhäusser, B., Thierfelder, N., Fang, Z., Khanin, R., and Rajewsky, N. (2008). Widespread changes in protein synthesis induced by microRNAs. *Nature* 455, 58–63.
- Shin, J., Berg, D.A., Zhu, Y., Shin, J.Y., Song, J., Bonaguidi, M.A., Enikolopov, G., Nauen, D.W., Christian, K.M., Ming, G.L., et al. (2015). Single-cell RNA-seq with waterfall reveals molecular cascades underlying adult neurogenesis. *Cell Stem Cell* 17, 360–372.
- Spalding, K.L., Bergmann, O., Alkass, K., Bernard, S., Salehpour, M., Huttner, H.B., Boström, E., Westerlund, I., Vial, C., Buchholz, B.A., et al. (2013). XDynamic of hippocampal neurogenesis in adult humans. *Cell* 153, 1219–1227.
- Spalding, K.L., Bhardwaj, R.D., Buchholz, B.A., Druid, H., and Frisén, J. (2005). Retrospective birth dating of cells in humans. *Cell* 122, 133–143.
- Stappert, L., Klaus, F., and Brüstle, O. (2018). MicroRNAs engage in complex circuits regulating adult neurogenesis. *Front. Neurosci.* 12, 707.
- Stricker, S.H., and Götz, M. (2018). DNA-methylation: master or slave of neural fate decisions? *Front. Neurosci.* 12, 5.
- Urban, N., and Guillemot, F. (2014). Neurogenesis in the embryonic and adult brain: same regulators, different roles. *Front. Cell. Neurosci.* 8, 396.
- van Battum, E.Y., Verhagen, M.G., Vangoor, V.R., Fujita, Y., Derijck, A.A.H.A., O'Duibhir, E., Giuliani, G., de Gunst, T., Adolfs, Y., Lelieveld, D., et al. (2017). An Image-Based miRNA screen identifies miRNA-135s as regulators of CNS axon growth and regeneration by targeting Krüppel-like factor 4. *J. Neurosci.* 38, 0662–717.
- van Praag, H. (2005). Exercise enhances learning and hippocampal neurogenesis in aged mice. *J. Neurosci.* 25, 8680–8685.
- van Praag, H., Kempermann, G., and Gage, F.H. (1999). Running increases cell proliferation and neurogenesis in the adult mouse dentate gyrus. *Nat. Neurosci.* 2, 266–270.
- Vizcaino, J.A., Deutsch, E.W., Wang, R., Csordas, A., Reisinger, F., Ríos, D., Dianas, J.A., Sun, Z., Farrah, T., Bandeira, N., et al.



- (2014). ProteomeXchange provides globally coordinated proteomics data submission and dissemination. *Nat. Biotechnol.* *32*, 223–226.
- Walker, T.L., Overall, R.W., Vogler, S., Sykes, A.M., Ruhwald, S., Lasse, D., Ichwan, M., Fabel, K., and Kempermann, G. (2016). Lysophosphatidic acid receptor is a functional marker of adult hippocampal precursor cells. *Stem Cell Reports* *6*, 552–565.
- Wu, H., Huang, M., Cao, P., Wang, T., Shu, Y., and Liu, P. (2012). MiR-135a targets JAK2 and inhibits gastric cancer cell proliferation. *Cancer Biol. Ther.* *13*, 281–288.
- Xu, B., Tao, T., Wang, Y., Fang, F., Huang, Y., Chen, S., Zhu, W., and Chen, M. (2016). hsa-miR-135a-1 inhibits prostate cancer cell growth and migration by targeting EGFR. *Tumor Biol.* *37*, 14141–14151.
- Zubieta, D.M.G., Hamood, M.A., Beydoun, R., Pall, A.E., and Kondapalli, K.C. (2017). MicroRNA-135a regulates NHE9 to inhibit proliferation and migration of glioblastoma cells. *Cell Commun. Signal.* *15*, 1–12.
- Zurawek, D., Kusmider, M., Faron-Gorecka, A., Gruca, P., Pabian, P., Solich, J., Kolasa, M., Papp, M., and Dziedzicka-Wasylewska, M. (2017). Reciprocal MicroRNA expression in mesocortical circuit and its interplay with serotonin transporter define resilient rats in the chronic mild stress. *Mol. Neurobiol.* *54*, 5741–5751.

Stem Cell Reports, Volume 12

Supplemental Information

MiR-135a-5p Is Critical for Exercise-Induced Adult Neurogenesis

Merixell Pons-Espinal, Caterina Gasperini, Matteo J. Marzi, Clarissa Braccia, Andrea Armirotti, Alexandra Pöttsch, Tara L. Walker, Klaus Fabel, Francesco Nicassio, Gerd Kempermann, and Davide De Pietri Tonelli

Figure S1 related to Figure 1

A

Target name	EXP1 Ct values		EXP2 Ct values		EXP3 Ct values	
	STD	RUN	STD	RUN	STD	RUN
miR-135a	24,142	32,448	20,975	21,225	19,784	19,696
miR-375	30,814	35,344	27,745	28,186	26,388	25,953
miR-203	32,996	34,865	28,829	29,491	27,756	27,136
miR-190	23,909	24,855	21,233	21,528	17,267	21,292
miR-381	29,31	29,699	25,307	25,398	25,04	24,774
miR-350	28,429	28,709	24,308	24,452	24,542	23,719
miR-340-3p	26,755	26,95	21,624	21,862	21,343	20,338
miR-31	29,469	29,351	25,332	26,311	23,661	23,305
Normalizers						
U87-001712	22,620	22,193	20,092	19,034	20,203	18,246
Y1-001727	22,126	21,635	19,849	20,545	18,988	17,653
snoRNA135-001230	22,995	22,45	13,905	14,005	14,403	12,984
snoRNA202-001232	16,457	16,336	20,2	19,495	19,845	18,458

B

Target name	STD1	STD2	STD3	RUN1	RUN2	RUN3	t-test (paired)
miR-135a	0,348	0,542	1,337	0,001	0,219	0,366	0,123
miR-190	0,003	0,005	0,014	0,000	0,002	0,005	0,113
miR-203	0,057	0,346	0,454	0,037	0,141	0,235	0,147
miR-375	0,409	0,453	7,653	0,158	0,178	0,121	0,383
miR-381	0,001	0,002	0,005	0,000	0,001	0,002	0,140
miR-350	0,010	0,027	0,035	0,006	0,012	0,011	0,130
miR-340-3p	0,018	0,054	0,049	0,011	0,023	0,023	0,100
miR-31	0,009	0,026	0,091	0,007	0,006	0,030	0,257

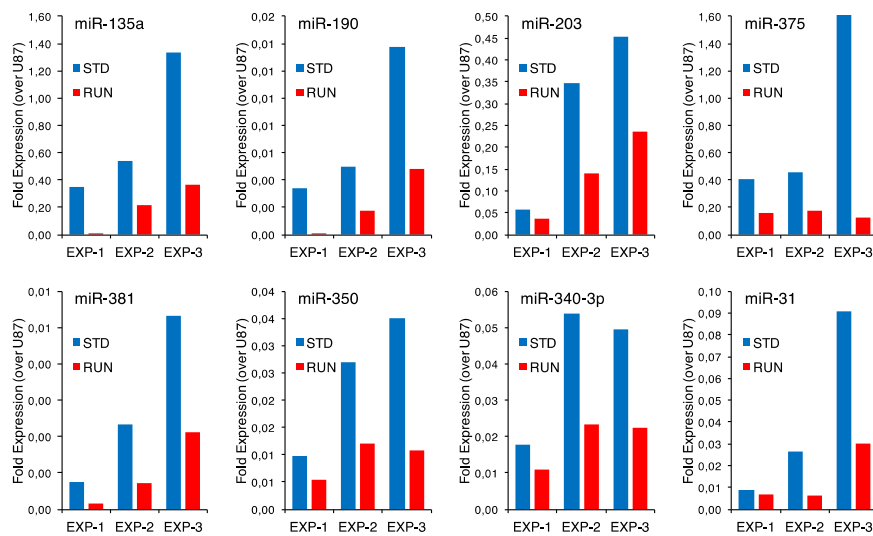


Figure S1. Fold change expression of miRNAs in *Nestin*-CFPnuc positive NPCs sorted from adult hippocampus of mice in standard (STD) or running (RUN) conditions for 10 days. (A) Expression levels of miRNAs and normalizers (Ct values) by TaqMan Low Density Array (TLDA) from each independent experiment (EXP; n=3 independent biological replicas each of them containing a pool of *Nestin*-CFPnuc positive cells isolated from 8 mice, per condition). (B) Normalized values from each independent experiment and plots.

Figure S2 related to Figure 3

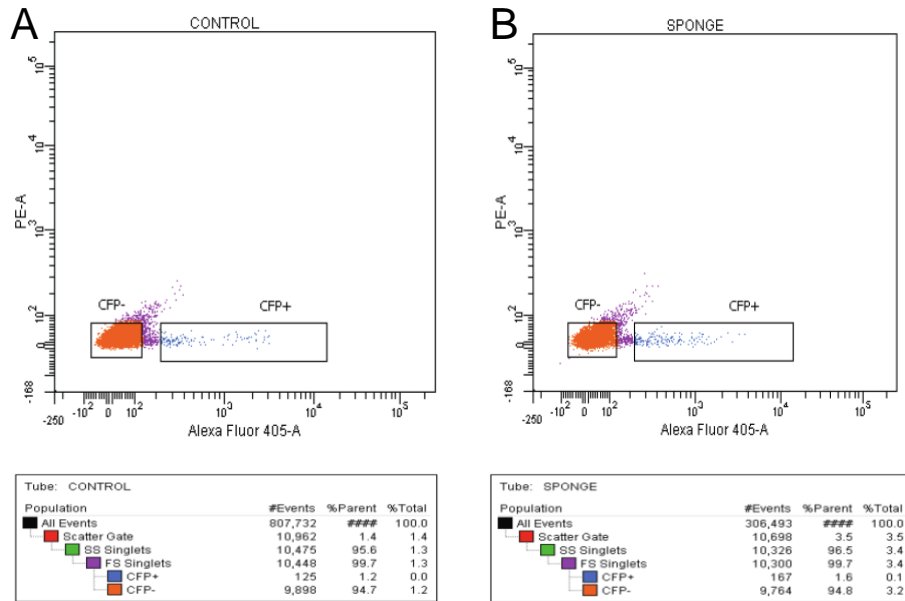


Figure S2. Inhibition of miR-135a increases the number of *Nestin*-CFPnuc positive NPCs *in vivo*. (A-B) Fluorescent sorting of CFPnuc positive cells from 6-week-old *Nestin*-CFPnuc mice after 10 days upon stereotaxic injections of lentiviruses encoding control (A), or miR-135a (B) sponge in the hippocampal DG of adult mice. n= 10 mice per group, pooled before sorting.

Figure S3 related to Figure 5

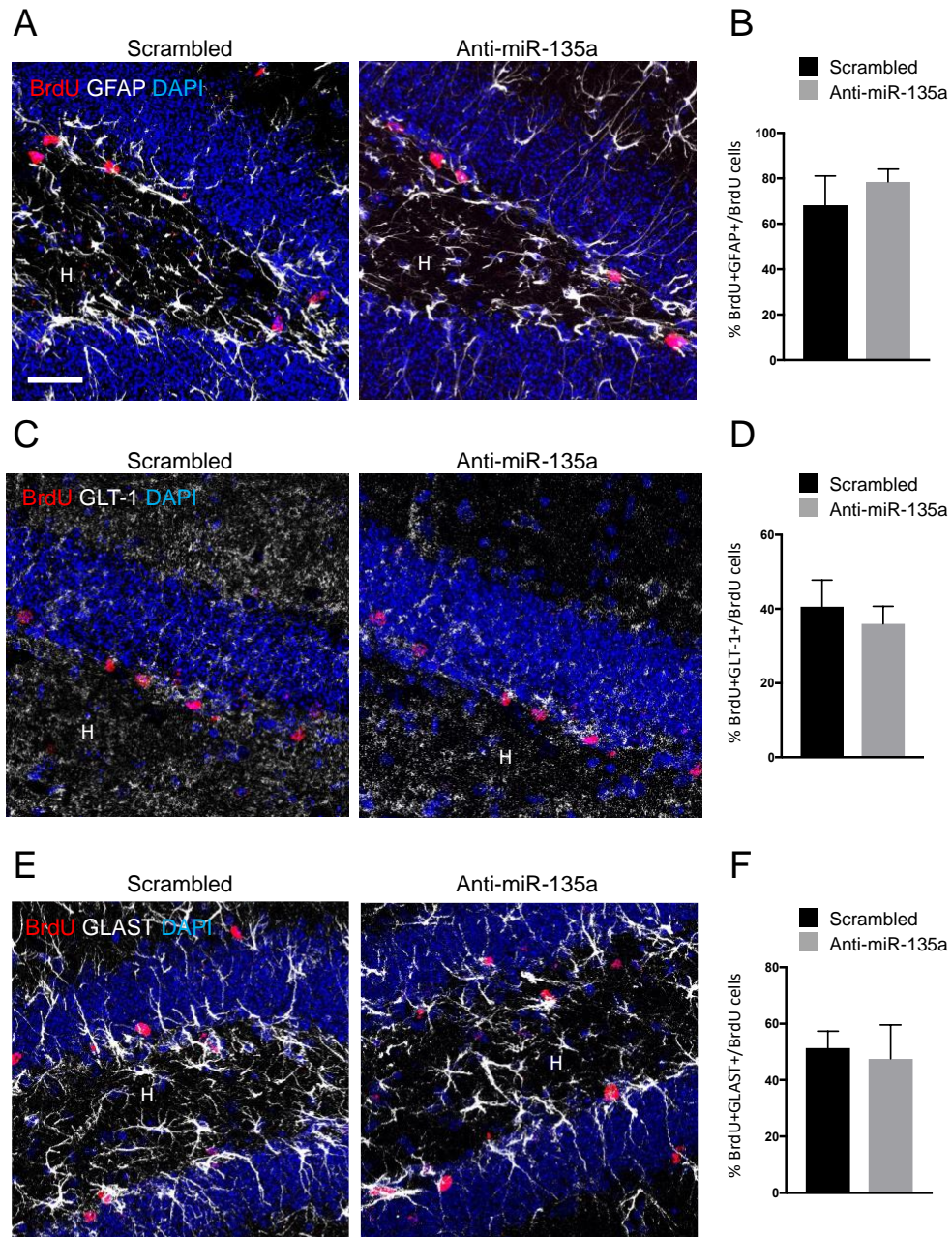


Figure S3. Transient inhibition of miR-135a does not alter the astroglial cell markers in hippocampal SGZ.

(A-F) Representative micrographs showing BrdU (red), GFAP (A), GLT-1 (C) or GLAST (E) (white) cells in hippocampal SGZ of 6-week-old C57BL/6 mice, injected with control scrambled or anti-miR-135a, subject to BrdU administration (2 injections every day per 5 days) and sacrificed 2 weeks after the last BrdU injection. (B) Quantification of the proportion BrdU+GFAP+ (B), BrdU+GLT-1+ (D) or BrdU+GLAST+ over total BrdU+ cells. H, hilus. Data are expressed as mean \pm SEM, n = 7 mice per group. Scale bars, 25 μ m.

Figure S4 related to Figure 6

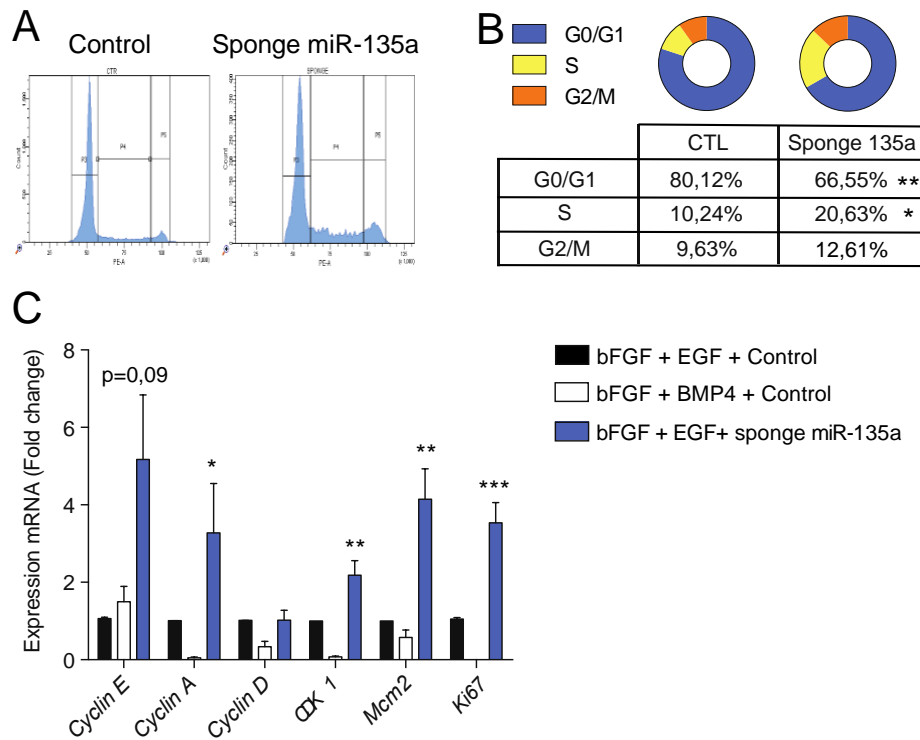


Figure S4. Downregulation of miR-135a regulates proliferation and cell cycle -dependent genes in NPCs *in vitro*.

(A) Representative cell cycle analysis of propidium iodide staining by flow cytometry. (B) Percentage of NPCs in G0/G1, S and G2/M phases upon infection with viral-encoded control or sponge for miR-135a *in vitro*. (C) Quantification of relative mRNA expression of cell cycle-dependent genes normalized to *Actin* in NPCs cultured in proliferative (bFGF+EGF), or quiescence (bFGF+BMP4) media upon transduction with viral-encoded control, and in proliferative media upon transduction with viral-encoded miR-135a sponge. Data are expressed as mean \pm SEM, n = 3 independent experiments containing three replicates. One-way ANOVA Bonferroni as post hoc. *p < 0.05, **p < 0.01, ***p < 0.001.

Table S1 related to Figure 1

miRNome expression analysis in *Nestin*-CFPnuc positive NPCs sorted from adult hippocampus of mice in standard (STD) or running (RUN) conditions for 10 days.

Table S2 related to Figure 6

Proteomics data upon miR-135a overexpression in NPCs *in vitro*.

Fold change of significantly differentially expressed proteins (cutoff > 1.5-fold or < 0.5-fold) and Gene ontology analysis, upon miR-135a overexpression (sh-miR-135a), compared to scrambled control. Blue and Red proteins indicate common protein found in both Table S2 and S3

Table S3 related to Figure 6

Proteomics data upon miR-135a inhibition in NPCs *in vitro*.

Fold change of significantly differentially expressed proteins (cutoff > 1.5-fold or < 0.5-fold) and Gene ontology analysis, upon miR-135a inhibition (sponge miR-135a) compared to scrambled control. Blue and Red proteins indicate common protein found in both Table S2 and S3

SUPPLEMENTAL EXPERIMENTAL PROCEDURES

Contact for reagent and resource sharing

“Further information and requests for resources and reagent should be directed to and will be fulfilled by the Lead Contact, Davide De Pietri Tonelli (davide.depietri@iit.it).

Primary NPC culture

Hippocampal NPCs were prepared and expanded as described previously from 8-10 6-week-old C57BL/6J mice (Babu et al., 2011) and kept in culture up to 10 passages (Pons-Espinal et al., 2017). Briefly, NPCs were plated into PDL/Laminin (Sigma/Roche) coated wells in culture medium containing Neurobasal (Invitrogen), Glutamax (Invitrogen), 1% penicillin and streptomycin (Invitrogen), B27 without retinoic acid (Invitrogen), bFGF (20ng/ml; PeproTech) and EGF (20ng/ml; PeproTech) and incubated at 37°C with 5% CO₂. Every 2 days half of the growth medium was exchanged with fresh medium to replenish the growth factors. NPCs were passaged once they reached 80% confluence.

To induce quiescence, 1.2×10^4 cells/cm² were plated into normal proliferation medium (EGF and bFGF, both at 20 ng/mL; PeproTech), and, after 16 h, fresh NPC medium was added without EGF and with 50 ng/mL BMP4 (R&D Systems) and 20 ng/mL bFGF (Martynoga et al., 2013).

Virus injection

8-week-old mice were anesthetized with isoflurane and 1.5 µl of virus per DG was stereotaxically injected at the following coordinates: -2.0 anterior/posterior, ±1.6 medial/lateral, and -1.9 to -2.1 dorsal/ventral relative to bregma (in millimeters) as previously described (Pons-Espinal et al., 2017). Virus used: *mmu-miR-135a-5p sponge*: MISSION® Lenti microRNA Inhibitor Mouse (MLTUD0048, Sigma); *mmu-miR-135a-5p overexpression*: MISSION® Lenti microRNA Human (HLMIR0200, Sigma) or *control lentivirus*: MISSION® TRC2 pLKO.5-puro Non-Mammalian shRNA Control (SHC202, Sigma). Mice were single-housed under standard conditions or in cages equipped with running wheels for 10 days. Mice received 3 BrdU intraperitoneal injections per day (100 mg/kg) (one every 2 hours) and sacrificed 24 hours later.

Histology: Mice were anesthetized with intraperitoneal administration of ketamine (90mg/kg) and xylazine (5-7mg/kg), and subsequently perfused with PBS followed by 4% paraformaldehyde (PFA). 40 µm brain sections were generated using a microtome and were stored with cryoprotectant solution.

Synthetic oligos injection

6-week-old mice were anesthetized with isoflurane and 1.5 µl of synthetic oligos per DG was stereotaxically injected at the following coordinates: -2.0 anterior/posterior, ±1.6 medial/lateral, and -1.9 to -2.1 dorsal/ventral relative to bregma (in millimeters) as previously described (Pons-Espinal et al., 2017). Oligos used: miRCURY LNA miRNA Custom Power Inhibitor I-MMU-MIR-135A-5P and NEGATIVE CONTROL (339146, Qiagen).

Mice were single-housed under standard conditions. To assess the effect of miR135 inhibition, a first group of mice (n=4) were sacrificed 48 hours after the injection and the DG dissected for RNA extraction and miR135 quantification. 24 hours after the oligos injection another set of animals received 2 BrdU intraperitoneal injections per day for 5 days (50 mg/kg) (one every 12 hours). 5 mice were then sacrificed 2 hours after the last BrdU injection and the remaining 7 were sacrificed 2 weeks after the last BrdU injection (in total, 21 days after oligos injection). Brains were collected as previously described and used for RNA extraction or immunofluorescence analysis.

MiRNA administration

MiRNA mimics (Qiagen): Syn-mmu-mir-135a-5p, MSY0000147; Syn-mmu-miR-203-3p, MSY0000236; or Syn-mmu-miR-190a-5p, MSY0000220.

MiRNA antagonists (Qiagen): Anti-mmu-miR-135a-5p, MIN0000147; Anti-mmu-miR-203-3p, MIN0000236; or Anti-mmu-miR-190a-5p, MIN0000220.

To constitutively overexpress or inhibit miR-135a-5p, NPCs were infected at MOI=5 with lentiviruses and selected with 1 µg/ml puromycin (Sigma). Cell cycle distribution was monitored by propidium iodide staining of cells and fluorescence-activated cell sorting (FACS).

Immunofluorescence

The immunofluorescence staining on brain slices was performed on sections covering the entire dorsal hippocampus (Bregma, -1.06 to -2.18 mm, Paxinos and Franklin, 2001). Sections were washed with 0.1M PBS during 40 min and pretreated with 2N HCL at 30,2°C for 30 min. After extensive washings with 0.1M PBS, sections were permeabilized with 0.3% PBS-T (PBS-Triton X-100) for 10 min followed with 20 min with 0.1% PBS-T.

To detect Ki67 immunostaining, citrate buffer 10 mM pH = 6 treatment during 10 min at 95 °C was used. Sections were blocked during 2 h with 0.1% PBS-T and 5% NGS at room temperature (RT) followed by incubation with primary antibodies in a blocking solution overnight at 4°C. The next day, after washing extensively with 0.1% PBS-T sections were subsequently incubated for 1 h with the corresponding secondary fluorescent antibodies (1/1000; Goat or donkey Alexa 488, 568, and 647nm, Invitrogen). Sections were counterstained with Hoechst (1:300), mounted and cover slipped with mowiol reagent.

The immunofluorescence staining on cell cultures was performed after fixing NPCs for 30 min with 4% paraformaldehyde (PFA) followed by extensive washings with PBS during 30 min. Cells were washed three times with PBS 0,1% Triton X-100 (PBS-T) and blocked during 2 hours with PBS-T containing 5% normal goat serum (Vector laboratories), followed by overnight incubation with primary antibodies. To detect BrdU incorporation, cells were pretreated with 2M HCl for 30 min at 37°C followed by washing with borate buffer, pH 8.5, for 30 min, before being subjected to immunofluorescence. The next day, after washing extensively with PBS-T, cells were incubated with secondary antibodies. Cells were mounted in mounting medium and counterstained with fluorescent nuclear dye DAPI (Invitrogen).

List of antibodies used:

Antibody	Host	Company	Catalog	Dilution
BrdU	rat	Abcam	ab6326	1:200
KI67	rabbit	Abcam	ab15580	1:250
GFAP	rabbit	Dako	Z-0334	1:1000
GFP	chicken	Abcam	ab13970	1:500
GLAST	rabbit	Abcam	ab416	1:200
GLT-1	rabbit	Abcam	ab41621	1:200
DCX	rabbit	Abcam	ab18723	1:1000
NEUN	mouse	Millipore	MAB377	1:250

Confocal stack images of brain slices (40µm) were obtained with the Confocal A1 Nikon Inverted SFC with 40x objective and the Zeiss Spinning Disc with a 20x objective. Cell quantification and analysis was performed using NIS-Elements

software (Nikon) and ZenBlue (Zeiss). Given that the density of the positive cells was relatively low, for each stacked-confocal image we drew and measure the area of the DG following the position of the nuclei stained with DAPI and in that particular area we counted the positive cells. To obtain the number of cells in the volume, the density of positive cells was multiplied by the thickness of the slice (40 µm). Final cell number was corrected after checking along z-stack that no overlapping cells were counted twice.

Immunofluorescence on cell cultures was performed as previously described (Pons-Espinal et al., 2017). Images were obtained using the microscope Nikon Eclipse at 20x or 40x magnification and quantification was performed using a Cell-counter plugin in FIJI (Fiji is Just ImageJ).

Fluorescence-Activated Cell Sorting (FACS), RNA Extraction and Analysis

For RNA extraction and cDNA preparation, six to ten *Nestin*-CFPnuc mice per condition were euthanized at the indicated time points (animal facility MTZ Dresden). DG cells were dissociated with the Neural Tissue Dissociation Kit P (Miltenyi Biotec) and FACS-sorted cells were immediately processed for RNA extraction (Walker et al., 2016). Total RNA was extracted with QIAzol protocol (Qiagen) and RNA purified with RNeasy Mini Kit, or miRNeasy Mini Kit (Qiagen) following the manufacturer's instructions. cDNA (for mRNAs) synthesis was obtained with ImProm-II reverse transcriptase (Promega); cDNA (from miRNA) was prepared with an miScript II RT kit using the HiSpec Buffer (Qiagen) according to the manufacturer's instructions. mRNA was quantified with a QuantiFast SYBR Green PCR Kit (Qiagen) on a ABI-7500 Real-Time PCR System (Applied Biosystems). Each sample was normalized to Actin levels. MiRNAs were quantified with the miScript SYBR Green PCR kit (Qiagen) following the manufacturer's recommendations on an ABI-7500 Real-Time PCR System (Applied Biosystems) or with TaqMan Array Rodent MicroRNA A Cards Set v3.0 (Thermo Fisher) following the manufacturer's recommendations with a ViiA 7 Real-Time PCR system (Thermo Fisher), for which original Ct values are available on request.

List of specific primers used:

Primer name	Sequence (5'-3')
Actin Fw	GGCTGTATTCCCCTCCATCG
Actin Rv	CCAGTTGGTAACAATGCCATGT
Ki67 Fw	ATTCAGTTCGCCAATCC
Ki67 Rv	GGCTCCGTCTTCATACCTAAA
Cyclin E Fw	GATCCAGAAAAAGGAAGGCAAA
Cyclin E Rv	TGAAGAAATTGCCAAGATTGACA
Cyclin A Fw	GCCTTCACCATTCATGTGGAT
Cyclin A Rv	TTGCTGCGGGTAAAGAGACAG
Cyclin D Fw	GCGTACCCTGACACCAATCTC
Cyclin D Rv	CTCCTCTTCGCACTTCTGCTC
CDK1 Fw	CAGAGCTGGCGACCAAGAA
CDK1 Rv	GATTGACCAGCTCTTCAGGATCTT
Mcm2 Fw	ATCCACCACCGCTTCAAGAAC
Mcm2 Rv	TACCACCAAACCTCTCACGGTT

***In situ* hybridization**

Mice were anesthetized and perfused transcardially with cold 4% paraformaldehyde in 1X PBS. Brains were removed and post-fixed in the same fixative for 5 hours at 4°C. Tissues were washed several times in 1X PBS prior to de-hydration with 30% sucrose in 1X PBS, overnight (or until they sink) at 4°C and carefully dried before proceeding with the flash freezing protocol: tissues were placed in a metal beaker filled with isopentane (Sigma), located in a foam cooler or laboratory ice bucket and surrounded with crushed dry ice. 18-20 µm brain slices were collected using a cryostat and attached on glass slides. Slices were permeabilized by treating twice for 10 min with RIPA buffer (NaCl 150 mM, NP-40 1%, Na deoxycholate 0.5%, SDS 0.1%, EDTA 1 mM, Tris pH 8.0 50 mM) and post-fixed for 10 min in 4% PFA in 1X PBS, followed by washes in 1X PBS to remove the excess PFA. The positive charges in the tissue were blocked by treating slides for 15 min with acetic anhydride (Sigma) (0.25% final concentration) in triethanolamine buffer (triethanolamine 100 mM, acetic acid pH 8.0), followed by washes with 1X PBS. In order to block aspecific sites, a pre-hybridization step with 200-250 µl hybridization solution (Formamide 50%, SSC 5X, Denhardts 5X, Salmon sperm DNA (500 µg/ml, yeast RNA 250 µg/ml) was carried out. After 1 hour, a hybridization solution containing 160 nM (miR135, miR190, miR203) or 100 nM (miR9) of the DIG-labeled LNA probe (Exiqon) was added and incubated ON. The next day, slides were washed for 1 hour with a post-hybridization solution (Formamide 50%, SSC 2X, Tween-20 0.1%). For the immunological detection, slides were incubated twice for 5 min and once for 20 min at RT in buffer B1 (Maleic acid 100 mM pH 7.5, NaCl 100mM, Tween-20 0.1%) and then blocked in buffer B2 (10% Normal Goat Serum in B1) for 1 hour. The anti-DIG antibody (Roche) was diluted 1:2000 in B2 buffer and incubated ON at 4°C. For development of the color reactions, two different alkaline phosphatase substrates were used: NBT/BCIP (Roche) or Fast Red TR/Naphthol AS-MX solution (Sigma), according to manufacturer instructions. The reaction was stopped by several washes with 0.1 % Tween 20 in 1X PBS. Sections were mounted using mounting resins (Thermo Fisher) or in VECTA-Shield mounting medium (VECTOR Labs) including DAPI, and imaged using conventional bright-field microscopy or a confocal microscope with the Cy-3 filter.

Proteomics

Chemicals and solvents were purchased from Sigma Aldrich (Milano, Italy), unless otherwise indicated. The NanoAcquity LC system, trapping column and Oasis SPE columns were purchased from Waters (Milford, MA, USA). The 5600+ TripleTof system, ProteinPilot, MarkerView softwares and the PepCalMix reference standard were purchased from SCIEX (Ontario, Canada).

Sample preparation and ion library creation: The ion library preparation has been previously described (Braccia et al., 2018).

Protein digestion for Sequential window acquisition of all theoretical (SWATH) mass spectra: The volume corresponding to 50 µg of proteins from each sample was incubated in 100 mM dithiothreitol (DTT) in ammonium bicarbonate 50 mM, for reduction of disulfide bonds and then alkylated with iodoacetamide (IAA). Protein content was precipitated with cold acetone. The resulting protein pellets were dried under a nitrogen stream and then dissolved in ammonium bicarbonate 50 mM. An overnight digestion was performed using trypsin. The resulting peptides were desalted on Pierce C18 Spin columns (Thermo scientific, USA), according to manufacturer's instructions. The desalted peptides were dried in a vacuum centrifuge.

LC-MS/MS analysis: Adult hippocampal NPC tryptic digests were re-dissolved in 3% ACN with 0.1% FA. As internal standard for retention time calibration, 5 µl of PepCalMix (corresponding to 250 pmoles) were spiked into each fraction. 2 µg of digest from each sample was acquired in SWATH mode (10.1038/sdata.2014.31, doi: 10.1002/pmic.201400270.) using a pre-acquired, dedicated ion library, as already described by our group (Braccia et al., 2018). For SWATH

quantification, the following criteria were set: minimum peptide confidence 90%, 50 ppm maximum mass tolerance, 30 minutes maximum RT tolerance, 6 MRM transitions per peptide and modified peptides were allowed. With these settings, we were able to quantify 3352 proteins from all the samples at 1% FDR. All the RAW data files used for protein quantification are freely available through the acquired for the present work are freely available through ProteomExchange database (Vizcaino et al., 2014, Deutsch et al., 2017) with identifier PXD009845.

Statistical analysis

Data are presented as mean \pm SEM and were analyzed using Prism 6 (GraphPad). Statistical details of experiments can be found in the Results and Figure legend sections. Statistical significance was assessed with a two-tailed unpaired *t test* for two experimental groups. For experiments with three or more groups, one-way ANOVA with Bonferroni's multiple comparison test as *post hoc* was used. Mean differences were considered to be statistically significant when $p < 0.05$.